

# Journal Pre-proof



A delicate balance between antibody evasion and ACE2 affinity for Omicron BA.2.75

Jiandong Huo, Aiste Dijokaite-Guraliuc, Chang Liu, Raksha Das, Piyada Supasa, Muneeswaran Selvaraj, Rungtiwa Nutalai, Daming Zhou, Alexander J. Mentzer, Donald Skelly, Thomas G. Ritter, Ali Amini, Sagida Bibi, Sandra Adele, Sile Ann Johnson, Neil G. Paterson, Mark A. Williams, David R. Hall, Megan Plowright, Thomas A.H. Newman, Hailey Hornsby, Thushan I. de Silva, Nigel Temperton, Paul Klenerman, Eleanor Barnes, Susanna J. Dunachie, Andrew J. Pollard, Teresa Lambe, Philip Goulder, OPTIC consortium, ISARIC4C consortium, Elizabeth E. Fry, Juthathip Mongkolsapaya, Jingshan Ren, David I. Stuart, Gavin R. Screaton

PII: S2211-1247(22)01802-2

DOI: <https://doi.org/10.1016/j.celrep.2022.111903>

Reference: CELREP 111903

To appear in: *Cell Reports*

Received Date: 14 September 2022

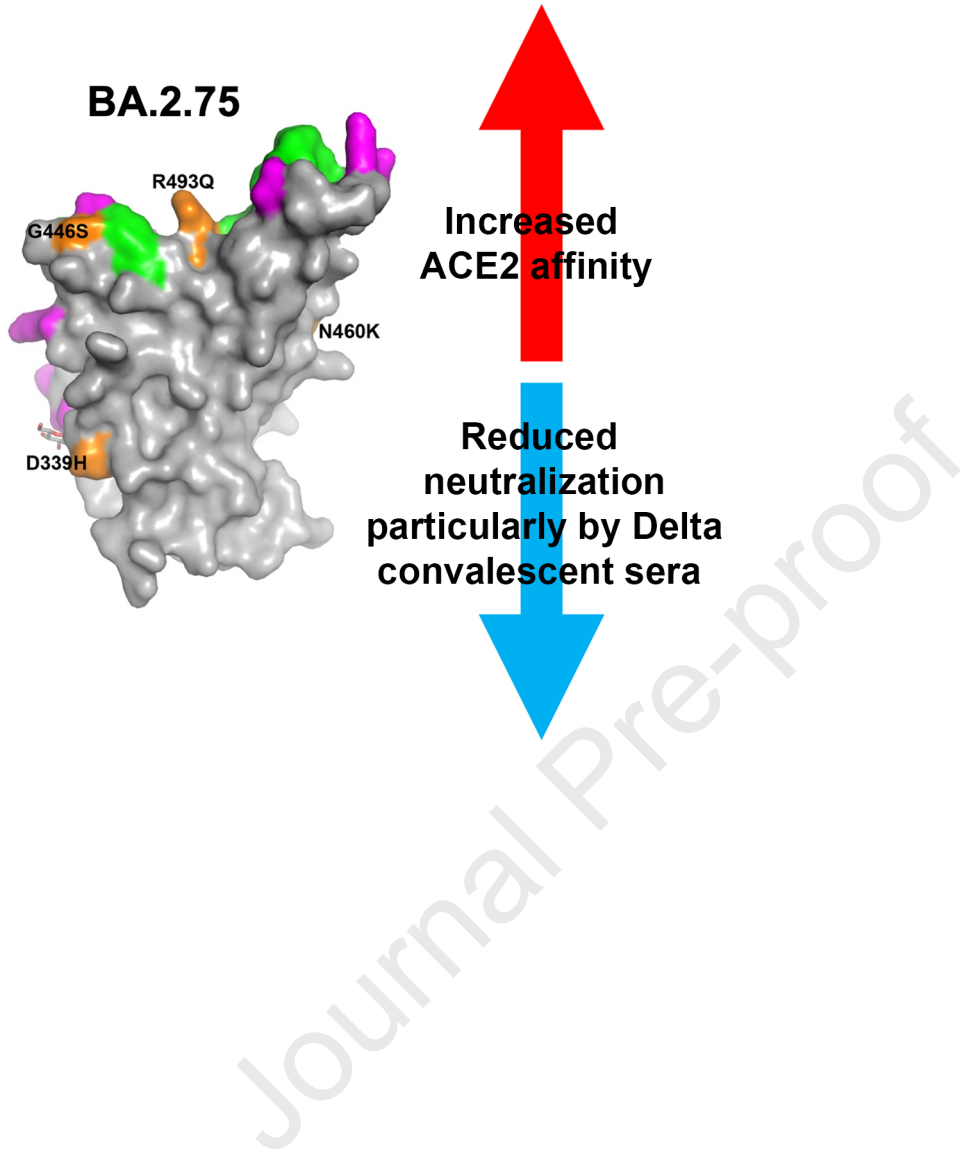
Revised Date: 5 November 2022

Accepted Date: 8 December 2022

Please cite this article as: Huo, J., Dijokaite-Guraliuc, A., Liu, C., Das, R., Supasa, P., Selvaraj, M., Nutalai, R., Zhou, D., Mentzer, A.J., Skelly, D., Ritter, T.G., Amini, A., Bibi, S., Adele, S., Johnson, S.A., Paterson, N.G., Williams, M.A., Hall, D.R., Plowright, M., Newman, T.A.H., Hornsby, H., de Silva, T.I., Temperton, N., Klenerman, P., Barnes, E., Dunachie, S.J., Pollard, A.J., Lambe, T., Goulder, P., OPTIC consortium, ISARIC4C consortium, Fry, E.E., Mongkolsapaya, J., Ren, J., Stuart, D.I., Screaton, G.R, A delicate balance between antibody evasion and ACE2 affinity for Omicron BA.2.75, *Cell Reports* (2023), doi: <https://doi.org/10.1016/j.celrep.2022.111903>.

This is a PDF file of an article that has undergone enhancements after acceptance, such as the addition of a cover page and metadata, and formatting for readability, but it is not yet the definitive version of record. This version will undergo additional copyediting, typesetting and review before it is published in its final form, but we are providing this version to give early visibility of the article. Please note that, during the production process, errors may be discovered which could affect the content, and all legal disclaimers that apply to the journal pertain.

© 2022



1 **A delicate balance between antibody evasion and ACE2 affinity for Omicron BA.2.75**

2

3 Jiandong Huo<sup>1,2,3,#,\*</sup>, Aiste Dijokaite-Guraliuc<sup>4,#</sup>, Chang Liu<sup>4,5,#</sup>, Raksha Das<sup>4</sup>, Piyada Supasa<sup>4</sup>,  
 4 Muneeswaran Selvaraj<sup>4</sup>, Rungtiwa Nutalai<sup>4</sup>, Daming Zhou<sup>2,5</sup>, Alexander J. Mentzer<sup>4,7</sup>, Donal  
 5 Skelly<sup>7,8,9</sup>, Thomas G. Ritter<sup>7</sup>, Ali Amini<sup>7,8,10</sup>, Sagida Bibi<sup>11</sup>, Sandra Adele<sup>7</sup>, Sile Ann Johnson<sup>7</sup>, Neil  
 6 G. Paterson<sup>6</sup>, Mark A. Williams<sup>6</sup>, David R. Hall<sup>6</sup>, Megan Plowright<sup>12,13</sup>, Thomas A.H. Newman<sup>12,13</sup>,  
 7 Hailey Hornsby<sup>12</sup>, Thushan I de Silva<sup>12,13</sup>, Nigel Temperton<sup>14</sup>, Paul Klenerman<sup>7,8,10,15</sup>, Eleanor  
 8 Barnes<sup>7,8,10,15</sup>, Susanna J. Dunachie<sup>7,8,16,17</sup>, Andrew J Pollard<sup>11,15</sup>, Teresa Lambe<sup>5,11</sup>, Philip  
 9 Goulder<sup>8,18</sup>, OPTIC consortium<sup>&</sup>, ISARIC4C consortium<sup>§</sup>, Elizabeth E. Fry<sup>2\*</sup>, Juthathip  
 10 Mongkolsapaya<sup>4,5,\*</sup>, Jingshan Ren<sup>2,\*</sup>, David I. Stuart<sup>2,5,6,\*^</sup>, Gavin R Screaton<sup>4,5,\*</sup>

11

12 1. State Key Laboratory of Respiratory Disease, National Clinical Research Center for Respiratory  
 13 Disease, Guangzhou Institute of Respiratory Health, the First Affiliated Hospital of Guangzhou  
 14 Medical University, Guangzhou, Guangdong, China

15 2. Division of Structural Biology, Nuffield Department of Medicine, University of Oxford, The  
 16 Wellcome Centre for Human Genetics, Oxford, UK

17 3. Guangzhou Laboratory, Bio-island, Guangzhou 510320, China

18 4. Wellcome Centre for Human Genetics, Nuffield Department of Medicine, University of Oxford,  
 19 Oxford, UK

20 5. Chinese Academy of Medical Science (CAMS) Oxford Institute (COI), University of Oxford,  
 21 Oxford, UK

22 6. Diamond Light Source Ltd, Harwell Science & Innovation Campus, Didcot, UK



- 23 7. Oxford University Hospitals NHS Foundation Trust, Oxford, UK
- 24 8. Peter Medawar Building for Pathogen Research, Oxford, UK
- 25 9. Nuffield Department of Clinical Neurosciences, University of Oxford, Oxford, UK
- 26 10. Translational Gastroenterology Unit, University of Oxford, Oxford, UK
- 27 11. Oxford Vaccine Group, Department of Paediatrics, University of Oxford, Oxford, UK
- 28 12. Department of Infection, Immunity and Cardiovascular Disease, University of Sheffield,
- 29 Sheffield, UK
- 30 13. Sheffield Teaching Hospitals NHS Foundation Trust, Sheffield, UK
- 31 14. Viral Pseudotype Unit, Medway School of Pharmacy, University of Kent and Greenwich
- 32 Chatham Maritime, Kent ME4 4TB, UK
- 33 15. NIHR Oxford Biomedical Research Centre, Oxford, UK
- 34 16. Centre For Tropical Medicine and Global Health, Nuffield Department of Medicine, University
- 35 of Oxford, Oxford, UK
- 36 17. Mahidol-Oxford Tropical Medicine Research Unit, Bangkok, Thailand, Department of
- 37 Medicine, University of Oxford, Oxford, UK
- 38 18. Department of Paediatrics, University of Oxford, Oxford, UK.

39 # These authors contributed equally to this work.

40 &,\$ See acknowledgements

41 \* Corresponding authors: huojiandong@gird.cn, liz@strubi.ox.ac.uk,  
42 juthathip.mongkolsapaya@well.ox.ac.uk, ren@strubi.ox.ac.uk, dave@strubi.ox.ac.uk,  
43 gavin.screaton@medsci.ox.ac.uk

44 ^ Lead contact

## 45 Summary

46 Variants of SARS CoV-2 have caused successive global waves of infection. These variants, with  
47 multiple mutations in the spike protein are thought to facilitate escape from natural and  
48 vaccine-induced immunity and often increase in the affinity for ACE2. The latest variant to  
49 cause concern is BA.2.75, identified in India where it is now the dominant strain, with evidence  
50 of wider dissemination. BA.2.75 is derived from BA.2 and contains four additional mutations in  
51 the receptor binding domain (RBD). Here we perform an antigenic and biophysical  
52 characterization of BA.2.75, revealing an interesting balance between humoral evasion and  
53 ACE2 receptor affinity. ACE2 affinity for BA.2.75 is increased 9-fold compared to BA.2; there is  
54 also evidence of escape of BA.2.75 from immune serum, particularly that induced by Delta  
55 infection which may explain the rapid spread in India, where BA.2.75 is now the dominant  
56 variant. ACE2 affinity appears to be prioritised over greater escape.

57

## 58 Introduction

59 SARS-CoV-2, the causative agent of coronavirus disease 2019 (COVID-19), has caused a  
60 devastating global pandemic, resulting in more than half a billion reported cases (probably  
61 greatly underestimating the number of infections) and over 6.4 million deaths as of August 2022  
62 (<https://covid19.who.int/>). As a positive-strand RNA virus, although its replication machinery  
63 contains a proofreading exonuclease, SARS-CoV-2 has a high viral replication error rate<sup>1</sup>. This,  
64 combined with the massive scale of the pandemic and chronic infection in immunocompromised  
65 individuals<sup>2</sup>, has generated mutational changes that endow viral fitness. The Spike (S) gene in

66 particular is the site of intense mutational change and selection<sup>3</sup> and the encoded S protein, the  
67 major viral surface glycoprotein, is the principal antigenic target of all SARS-CoV-2 vaccines<sup>4</sup> and  
68 monoclonal antibody therapeutics<sup>5</sup> in current use.

69

70 S is presented as elongated trimeric spikes protruding from the virion surface. S is subdivided into  
71 an N-terminal S1 domain, responsible for host cell adhesion, and a C-terminal S2 domain  
72 anchored in the viral membrane, responsible for membrane fusion and cell entry after cleavage  
73 from S1, allowing the viral RNA to enter the host cell cytoplasm and initiate viral replication<sup>6</sup>. S1  
74 consists of an N-terminal domain (NTD) and the receptor binding domain (RBD) which mediates  
75 interaction with the ACE2 receptor on the host cell surface. Although a number of neutralising  
76 monoclonal antibodies (nmAbs) have been found to target the NTD, especially the NTD supersite<sup>7</sup>,  
77 the majority of the nmAbs, particularly the most potent broadly reactive, target the RBD<sup>8,9</sup>,  
78 including all those in clinical use<sup>10</sup>.

79

80 The RBD is thus under intense selective pressure, and mutational changes may endow the virus  
81 a fitness advantage by enhancing viral transmissibility via an increased binding affinity for ACE2<sup>11</sup>,  
82 or to evade the humoral response by impairing binding of the nmAbs to the RBD<sup>12</sup>. The rapid  
83 genetic evolution of SARS-CoV-2 raises an immediate need to monitor and characterize the  
84 transmissibility of new variants and their capacity for immune evasion.

85

86 A large number of variants have emerged, several of which have been designated variants of  
87 concern (VoC) ([https://www.cdc.gov/coronavirus/2019-ncov/variants/variant-](https://www.cdc.gov/coronavirus/2019-ncov/variants/variant-classifications.html)  
88 [classifications.html](https://www.cdc.gov/coronavirus/2019-ncov/variants/variant-classifications.html)). Some VoC have caused successive waves of infection worldwide: Alpha<sup>13</sup>,  
89 then Delta<sup>14</sup> and recently Omicron<sup>15</sup> whilst Beta<sup>16</sup> in Southern Africa and Gamma in South  
90 America<sup>17</sup> have caused regional outbreaks without widespread global spread.

91

92 Omicron has caused the largest number of infections in the UK, with over 2.6 million confirmed  
93 cases (including BA.1 and BA.2) reported ([https://www.gov.uk/government/publications/covid-](https://www.gov.uk/government/publications/covid-19-variants-genomically-confirmed-case-numbers/variants-distribution-of-case-data-17-june-2022)  
94 [19-variants-genomically-confirmed-case-numbers/variants-distribution-of-case-data-17-june-](https://www.gov.uk/government/publications/covid-19-variants-genomically-confirmed-case-numbers/variants-distribution-of-case-data-17-june-2022)  
95 [2022](https://www.gov.uk/government/publications/covid-19-variants-genomically-confirmed-case-numbers/variants-distribution-of-case-data-17-june-2022)). Over 30 mutations are found in Omicron S, including 15 substitutions in the RBD, leading  
96 to increased transmissibility<sup>18</sup> and widespread large reductions in neutralizing antibody titres<sup>15</sup>.

97

98 Soon after the identification of Omicron BA.1, a number of sublineages emerged; BA.1.1,  
99 containing an additional R346K mutation in RBD, at one point accounted for about 40% of  
100 Omicron sequences globally, and about 35–60% in the UK and the USA<sup>19</sup>, but was soon  
101 outcompeted by BA.2. BA.2 contains 8 unique substitutions in S, 6 within the RBD, and lacks 13  
102 mutations found in BA.1<sup>20</sup>, and has become the dominant strain across the world  
103 ([https://www.who.int/publications/m/item/weekly-epidemiological-update-on-covid-19---6-](https://www.who.int/publications/m/item/weekly-epidemiological-update-on-covid-19---6-july-2022)  
104 [july-2022](https://www.who.int/publications/m/item/weekly-epidemiological-update-on-covid-19---6-july-2022)). Recently, BA.2.12.1 has been identified in multiple countries  
105 (<https://www.who.int/en/activities/tracking-SARS-CoV-2-variants/>), and caused a large regional  
106 outbreak in North America (58% of sequences as of May 25, 2022)<sup>21</sup>. In April 2022, BA.4 and BA.5

107 (which have identical S sequences) were reported from South Africa and now account for the  
108 majority (particularly BA.5) of sequenced cases in many countries  
109 ([https://www.who.int/publications/m/item/weekly-epidemiological-update-on-covid-19---6-  
110 july-2022](https://www.who.int/publications/m/item/weekly-epidemiological-update-on-covid-19---6-july-2022)).

111  
112 In early May 2022, a new Omicron BA.2 sublineage designated BA.2.75 was reported in India  
113 (<https://www.who.int/en/activities/tracking-SARS-CoV-2-variants/>) and has spread to multiple  
114 countries, including the UK, US, Australia, Germany and Canada. Here, we report the antigenic  
115 characterisation of BA.2.75 in comparison to other Omicron sub-lineages. In India, confirmed  
116 cases of BA.2.75 have outcompeted BA.5 and increased steeply from less than 20% of the total  
117 in early July to nearly 70% in mid-August ([https://cov-  
118 spectrum.org/explore/India/AllSamples/from=2022-07-01&to=2022-08-  
119 21/variants?variantQuery=nextcladePangoLineage%3ABA.2.75\\*&](https://covid.spectrum.org/explore/India/AllSamples/from=2022-07-01&to=2022-08-21/variants?variantQuery=nextcladePangoLineage%3ABA.2.75*&)). We find that neutralisation  
120 of BA.2.75 is reduced compared to BA.2 using a number of vaccine and immune sera, but  
121 reductions are not as great as those found with BA.4/5. However, sera from Delta infected cases  
122 showed no neutralization of BA.2.75 which may underlie the evolution and emergence of BA.2.75  
123 in India which suffered a major Delta wave in 2021. Finally, perhaps the most striking change  
124 found in BA.2.75 is the affinity of ACE2/RBD interaction. BA.2.75 affinity is increased 9-fold  
125 compared to BA.2. BA.2.75 has the highest affinity of all the SARS-CoV-2 variants measured to  
126 date and the only sub-nanomolar affinity we have determined. The N460K mutation probably  
127 increases affinity for ACE2 and also reduces the binding of some potent neutralising antibodies.  
128 However, affinity to ACE2 appears to be prioritised over neutralisation escape, as evidenced by

129 the acquisition of the RBD reversion mutation R493Q, which increases ACE2 affinity, but makes  
130 the virus more sensitive to neutralization by vaccine sera. The very high affinity of BA.2.75 for  
131 ACE2 may increase the transmissibility of BA.2.75.

132

## 133 **Results**

### 134 *The Omicron lineage BA.2.75*

135 BA.2.75 contains multiple mutational changes in the S protein compared to BA.2, including four  
136 substitutions in the NTD (W152R, F157L, I210V and G257S) and four in the RBD: D339H, G446S,  
137 N460K and R493Q (**Figure 1**). The RBD mutations impinge on major epitopes for neutralising  
138 antibodies and are likely to modulate ACE2 binding. D339H represents a further evolution of the  
139 G339D mutation found in all previous Omicron variants that has been found to impair the binding  
140 of certain 'right-flank' antibodies belonging to the IGHV1-69 family (e.g. Beta-49 and -50) and  
141 falls in the binding footprint of certain Class 3 antibodies such as S309/sotrovimab<sup>15</sup>. G446S was  
142 found in BA.1, BA.1.1 and BA.3 but not in BA.2 and other BA.2 subvariants, and is also able to  
143 impair binding of certain Class 3 antibodies binding the right shoulder such as REGN10987/  
144 imdevimab<sup>15</sup>. The R493Q reversion was also found in BA.4/5, and may make the virus more  
145 sensitive to neutralization by a number of class 1 and 2 antibodies binding the neck/left shoulder.  
146 This reversion may also increase the affinity for ACE2 (see below).

147

148 N460K is a mutation not seen in previous VoC or Omicron sublineages, but it was found after *in*  
149 *vitro* (yeast display) evolution in RBD-62 which has an ultra-high ACE2 affinity (KD = 16-18 pM)<sup>15,11</sup>.  
150 N460K was found repeatedly in these screens and is presumed to increase affinity for ACE2<sup>11</sup>.  
151 Furthermore, our *in silico* analysis (below) suggests that N460K affects the binding of certain  
152 antibodies belonging to the IGHV3-53/66 families, which have been shown to be able to potently  
153 neutralise all VoC<sup>20</sup>.

154

#### 155 *Neutralisation of BA.2.75 by vaccine serum*

156 We constructed a panel of pseudotyped lentiviruses<sup>22</sup> expressing the S gene from the Omicron  
157 sub-lineages BA.1, BA.1.1, BA.2, BA.2.12.1, BA.4/5, BA.2.75, together with Victoria, an early  
158 pandemic Wuhan related strain, used as control. We also included D339H, G446S, N460K and  
159 R493Q as single mutations on the BA.2 background. Neutralization assays were performed using  
160 serum obtained 28 days following a third dose of the Oxford-AstraZeneca vaccine AZD1222 (n =  
161 41)<sup>23</sup> or of Pfizer-BioNtech vaccine BNT162b2 (n = 22)<sup>24</sup> (**Figure 2**).

162

163 For BNT162b2, neutralization of BA.2.75 was reduced 1.3-fold compared to BA.2 (p=0.0359), but  
164 increased 2.2-fold compared to BA.4/5 (p<0.0001) (**Figure 2A**). For AZD1222, neutralization of  
165 BA.2.75 was reduced 1.2-fold compared to BA.2 (p=0.0182) and 1.1-fold compared to BA.2.12.1  
166 (p=0.0065), but increased 1.5-fold compared to BA.4/5 (p<0.0001) (**Figure 2B**). Overall, there are  
167 modest reductions in BA.2.75 neutralization titres of vaccine serum compared to BA.2 but not to  
168 the level seen with BA.4/5.

169

170 *Neutralization of BA.2.75 by serum from vaccine breakthrough BA.1, BA.2 or BA.4/5 infections*

171 Breakthrough BA.1 serum samples were taken from vaccinated volunteers  $\geq 28$  days from  
172 symptom onset (median 38 days; n=16). Pseudoviral neutralization assays were performed  
173 against the panel of pseudoviruses described above (**Figure 2C**). Neutralisation titres for BA.2.75  
174 were similar to BA.2, and 1.4-fold (p=0.0052) and 2.0-fold (p=0.0001) higher than BA.2.12.1 and  
175 BA.4/5 respectively.

176

177 Breakthrough BA.2 serum samples were taken from vaccinated volunteers  $\geq 12$  days from  
178 symptom onset (median 29 days; n=23). Pseudoviral neutralization assays were performed  
179 against the panel of pseudoviruses: Victoria, BA.1, BA.1.1, BA.2, BA.2.12.1, BA.4/5 and BA.2.75  
180 (**Figure 2D**). Here, neutralization titres against BA.2.75 were modestly reduced compared to BA.2  
181 (1.4-fold; P=0.0021), similar to BA.2.12.1, but still higher than BA.4/5 (0.7-fold; P=0.0123). Taken  
182 together, BA.2.75 shows a modest degree of escape from humoral response induced by BA.2  
183 breakthrough infection but not BA.1 infection.

184

185 Sequence confirmed BA.4/5 infection serum samples were taken from 11 individuals (all but one  
186 vaccinated)  $> 14$  days (median = 38 days) (**Figure 2E**). Neutralization titres to BA.2.75 were 1.6-  
187 fold (p=0.0186) reduced compared to BA.2 and reduced, but not significantly, in this relatively  
188 small sample compared to BA.4/5. These results are in line with the fact that the four new



189 mutations found in BA.2.75 RBD are not shared with BA.2 or BA.4/5. Interestingly, although only  
190 a single case, the outlier on Figure 2E, essentially no neutralization of BA.1.1 (<50% neutralization  
191 at 1:20 serum dilution), and a low titre to BA.2.75 (7.7-fold reduced compared to BA.4/5) was  
192 from the unvaccinated case in this series; if this was representative of the response in the  
193 unvaccinated, it would suggest that unvaccinated individuals may be more susceptible to BA.2.75  
194 infection following BA.4/5 infection.

195 .

#### 196 *Individual BA.2.75 mutation have differential effects on neutralization*

197 To understand the effects of the individual mutations in the BA.2.75 RBD we introduced them  
198 individually into the pseudovirus BA.2 background and assayed their neutralization using triple  
199 vaccinated Pfizer BNT162b2 serum (**Figure 2F**). Neutralization titres for BA.2 were reduced for 3  
200 of the 4 single mutation variants of BA.2, with the greatest decrease for N460K (2.9-fold,  
201  $p < 0.0001$ ), followed by D339H (1.3-fold,  $p = 0.0006$ ), then by G446S (1.2-fold,  $p = 0.2312$ ), however  
202 neutralization titres were increased 1.5-fold by the R493Q reversion mutation ( $p < 0.0001$ ). Q493  
203 is present in all vaccines thus explaining the increase in activity of vaccine serum to this reversion  
204 mutation.

205

#### 206 *ACE2/RBD binding affinities*

207 We used surface plasmon resonance (SPR) to characterise the interaction between ACE2 and the  
208 BA.2.75 RBD. The off-rate is slow, leading to a sub-nanomolar affinity (BA.2.75/ACE2  $K_D = 0.45$

209 nM) (**Figures 3A, B**). This represents a considerable increase in affinity compared to BA.2 (9-fold)  
210 (**Figure 3C**), and is even tighter than BA.4/5 (5-fold) (**Figure 3D**), which was previously shown to  
211 bind ACE2 with higher affinity than BA.2<sup>12</sup>. Indeed, BA.2.75 is the strongest ACE2 binder amongst  
212 all SARS-CoV-2 VoC, including Alpha (Alpha/ACE2 KD = 1.5 nM; (**Figure 3E**), and is the only sub-  
213 nanomolar affinity we have measured. We were unable to express BA.2+N460K RBD which is  
214 expected to contribute to the increased affinity, but we measured the binding affinity of  
215 BA.2+R493Q RBD to ACE2 (KD = 0.55 nM) (**Figure 3F**), confirming that the reversion mutation  
216 contributes to the high affinity of BA.2.75 RBD.

217

#### 218 *ACE2/BA.2.75 RBD structure*

219 To elucidate the molecular mechanism for high affinity, we determined the structure of the  
220 BA.2.75 RBD with ACE2 by crystallography (see Methods). As expected the binding mode was  
221 essentially indistinguishable from that observed before (**Figure 4A**), although there were  
222 significant rearrangements outside of the ACE2 footprint, with the flexible RBD 371-375 loop re-  
223 arranging, and part of the C-terminal 6xHis tag becoming ordered. **Figure 4B**, shows a close-up  
224 of the binding interface, compared with the ACE2/BA.2 RBD complex. We note that in other  
225 complexes (with either R or Q at RBD 493) K31 of ACE2 tends to be disordered, whereas it is well  
226 ordered in the BA.2.75 complex, allowing K31 to form a potential hydrogen bond with the  
227 glutamine 493 sidechain of the RBD sidechain, possibly increasing the affinity of ACE2. Although  
228 N460K is outside of the footprint of ACE2 on the RBD (**Figure 4A**), evidence from in vitro evolution,  
229 suggests that it probably increases the affinity for ACE2<sup>11</sup>. This is probably due to the improved

230 electrostatic match<sup>11</sup>, although we also note that the density map for RBD-61 with ACE2<sup>11</sup>  
231 (EMDB:12187), suggests that the glycan attached to N90 of ACE2 makes a direct interaction with  
232 the RBD close to residue 460.

233

#### 234 *Escape from monoclonal antibodies by BA.2.75*

235 To dissect how BA.2.75 might affect neutralising antibody activity, we used pseudoviral assays to  
236 test a recently reported panel of potent human mAb generated from cases of Omicron  
237 breakthrough infection (BA.1 IC<sub>50</sub> titres < 0.1 µg/ml)<sup>20</sup> (**Figure 5A, Table S1A**). Among the 27  
238 RBD-specific mAbs, those belonging to the IGHV3-53/66 families are the most severely affected.  
239 Three (Omi-16, Omi-29 and Omi-36) showed a complete knock out of BA.2.75 neutralization; an  
240 additional four (Omi-18, Omi-20, Omi-27 and Omi-28) showed > 5-fold reduction compared to  
241 BA.2, which is in line with the observation that N460 interacts very closely with the highly  
242 conserved GGS/T CDR-H2 motif found in many IGHV-3/66 antibodies.

243

244 Structures for two representative mAbs, Omi3 and Omi-18, in **Figures 6A,B**<sup>17,14,20</sup>, indicate that  
245 the larger lysine side-chain of the N460K mutation will interfere with binding. Like BA.2 and  
246 BA.4/5, BA.2.75 is not neutralised by the anti-NTD mAb Omi-41, which only interacts with the  
247 NTD of BA.1, BA.1.1 and BA.3.

248

249 The Omi mAbs were also tested against the pseudoviruses encoding single point mutations in the  
250 BA.2 RBD described above (**Figure S1, Table S2**). As expected, the VH3-53/66 mAbs that lost  
251 neutralization to BA.2.75 were also impacted by the N460K mutation, confirming the prediction  
252 that this residue was critical for the binding of a number of this public gene family. Interestingly,  
253 The BA.2+N460K mutation in isolation shows a larger impact than the full BA.2.75 complement  
254 of S mutations on the activity of several mAbs: the neutralisation titre of Omi-3 (IGHV3-53) was  
255 reduced 50-fold for BA.2+N460K but only 2-fold for BA.2.75; Omi-17 (IGHV3-66) was completely  
256 knocked out on BA.2+N460K but only reduced 4-fold for BA.2.75; and Omi-33 (IGHV3-33) was  
257 reduced 7-fold for BA.2+N460K but there was no change observed for BA.2.75. Thus, other  
258 mutations in BA.2.75 might have mitigated the effect of the N460K mutation, particularly the  
259 R493Q mutation, which has a different impact on various IGHV gene families, and even differs  
260 within the 3-53/66 family (**Figure 6C**). However, we cannot fully explain the marked differences  
261 of effect observed for the impact of the 460 mutation between Omi-3 and Omi-18 (**Figure S1,**  
262 **Table S2**), since the contacting GGS/T CDR-H2 motif is structurally almost identical between these  
263 two mAbs (**Figure 6B**). Interestingly, BA.2.75 is more sensitive to Omi-32 (IGHV-3-33) than is BA.2,  
264 with an 8-fold increase in neutralisation titre (**Figure 5A, Table S1**).

265

266 To confirm that the changes in neutralising activities observed are associated with alterations in  
267 RBD interaction, we performed binding analyses of selected antibodies to BA.2.75 and BA.2 RBDs  
268 by surface plasmon resonance (SPR) (**Figure S2**). Binding of Omi-29 (IGHV3-53) and Omi-36  
269 (IGHV3-66) to BA.2.75 was severely impaired, and Omi-18 and Omi-20 showed 8-fold reductions

270 compared to BA.2. On the other hand, a 2-fold increase in binding affinity of Omi-32 was seen for  
271 BA.2.75 in comparison with BA.2, in line with the enhanced neutralisation titre observed (above).

272

### 273 *Effect of commercial monoclonals against BA.2.75*

274 We evaluated the sensitivity of a panel of mAbs that have been developed as therapeutics against  
275 BA.2.75 (**Figure 5B, Table S1B**). The neutralisation profiles are in general similar between BA.2.75  
276 and BA.2; however, further to the 6/12 mAbs (REGN10933, ADG10, ADG20, ADG30, Ly-CoV555,  
277 Ly-CoV16) which have already suffered complete loss of neutralising activity for BA.2, the residual  
278 activity of REG10987<sup>25</sup> against BA.2 was further knocked out for BA.2.75 due to the G446S  
279 mutation<sup>15</sup>. For AZD1061, activity against BA.2.75 was similar to that against BA.2 (<3-fold  
280 reduction); whilst the AZD8895 titre was restored to 8 ng/ml for BA.2.75 from 1333 ng/ml for  
281 BA.2, a 167-fold increase in activity. As a result, AZD7442 (a combination of AZD8895 and  
282 AZD1061)<sup>26</sup> showed similar activity against BA.2.75 and BA.2 (2-fold reduction). The results can  
283 be explained by the structure of the ternary complex of the ancestral SARS-CoV-2  
284 RBD/AZD1061/AZD8895<sup>26</sup>. G446 has contacts with CDR-L2 Y55 and W56 of AZD1061 thus the  
285 G446S mutation will induce steric clashes (**Figures 6D, E**), while the CDR-H2 of AZD8895 sits above,  
286 and makes a hydrogen bond to Q493 of the RBD, an arginine at 493 will severely clash with the  
287 CDR-H2 (**Figures 6F, G**). The activity of S309<sup>27</sup> is increased 3-fold for BA.2.75 compared to BA.2,  
288 suggesting that the D339H mutation in BA.2.75 reduces the impact of the preceding G339D  
289 mutation in BA.2 on the activity of S309. LY-CoV1404 (bebtelovimab)<sup>28</sup> is the only mAb where  
290 neutralization is fully retained on all Omicron sublineages.

291

292 *Antigenic mapping*

293 We tested the neutralization of BA.2.75 using serum from previously infected individuals. This  
294 included serum obtained early in the pandemic (before the emergence of Alpha) together with  
295 sera obtained following Alpha, Beta, Gamma, Delta, BA.1 and BA.2 infection (**Figure S3**). As  
296 expected, BA.2.75 neutralization titres were lower than the homologous infecting strain (e.g.  
297 Alpha serum on the Alpha strain). Most striking however, was the complete loss of BA.2.75  
298 neutralization using Delta serum (zero samples achieved 50% neutralization at 1/20 dilution).  
299 However, titres to BA.2.75 were much higher in cases who had been vaccinated before or after  
300 Delta infection.

301

302 We used these data to place BA.2.75 onto a three-dimensional antigenic map using the method  
303 we have previously reported<sup>12</sup> (**Figures 7A, B and Videos S1, S2**). Initially, all VoC were included  
304 (**Figure 7A, Video S1**); BA.2.75 forms part of the constellation of Omicron viruses, which  
305 segregate into one hemisphere of the 3D plot. BA.2.75 is well separated from other Omicron sub-  
306 lineages and especially from BA.4/5. It is notable that BA.2.75 and Delta are diametrically  
307 opposed in the diagram, emphasising the antigenic distance between these two viruses. Since  
308 the data are higher dimensional, this 3D projection is likely to distort the true distances and so  
309 we re-calculated the map only for the Omicron lineage and early pandemic viruses (but retain  
310 the fully serology information for these). The results are shown in **Figure 7B, Video S2** and  
311 recapitulate the major features of the plot containing the other VoCs, but allow the Omicron sub-

312 lineages to distribute more broadly in 3D space. It is remarkable that if we consider the two early  
313 pandemic viruses as a single point, and likewise merge BA.2 and BA.3 pairs then the points are  
314 distributed as a trigonal bi-pyramid, maximising their separation, consistent with antigenic  
315 escape being a significant factor in their evolution.

316

## 317 **Discussion**

318 Following the designation of Omicron as a variant of concern in November 2021, a succession  
319 of sub-lineages emerged, including BA.1.1, BA.2, BA.2.12.1, BA.4/5, which have outcompeted  
320 preceding strains to become regionally or globally dominant. Since June 2022, BA.4/5, which has  
321 both higher receptor binding affinity and a markedly enhanced escape from antibody responses<sup>12</sup>,  
322 quickly spread from South Africa across the world and has now become the new globally  
323 dominant strain, with BA.5 in the ascendency in many regions.

324

325 Very recently, a new Omicron sub-lineage designated as BA.2.75 has emerged in India and spread  
326 to many countries. The true prevalence of BA.2.75 is difficult to determine as sequencing in many  
327 countries is patchy and has in recent months been greatly scaled back. However, in India BA.2.75  
328 has rapidly outcompeted BA.4/5 to recently become the dominant variant. Here, we show  
329 reductions in neutralization titres to BA.2.75 of triple-dosed BNT162b2 and AZD1222 vaccine  
330 serum compared to BA.2, but the reductions in BA.2.75 neutralization are less pronounced than  
331 BA.4/5. For serum derived from BA.1 breakthrough infection in vaccinated individuals, the  
332 BA.2.75 titres are similar to BA.2. However, we find BA.2.75 neutralisation titres are modestly

333 lower (1.3-fold) than BA.2 for BA.2 breakthrough serum and 1.6-fold reduced compared to BA.2  
334 for BA.4/5 infected serum and if the results on BA.2.75 neutralization by BA.4/5 from a single  
335 unvaccinated case were replicated on a larger scale it would suggest that such individuals would  
336 be more at risk of BA.2.75 infection.

337

338 Overall, the constellation of mutations in BA.2.75 compared to BA.2 have opposing effects on  
339 neutralization, the reversion mutation R493Q makes the virus easier to neutralize using vaccine  
340 serum (the vaccine contains Q493), whilst N460K reduces neutralization titres to a greater extent  
341 when expressed in isolation compared to the combination of mutations seen in BA.2.75. N460K  
342 is a substitution that has not appeared in preceding variants of SARS-CoV-2. When we introduced  
343 N460K into the BA.2 backbone BA.2+N460K titres were reduced 2.9-fold compared to BA.2,  
344 greater than the reduction seen with BA.2.75, and on a par with the reduction seen for BA.4/5,  
345 using BNT162b2 triple vaccinated serum.

346

347 Dissecting these effects using a panel of potent mAbs derived from vaccinated individuals who  
348 suffered BA.1 vaccine breakthrough infection, we show that those belonging to the IGHV3-53/66  
349 family are reduced or knocked out against BA.2.75. IGHV3-53/66 are the most frequently isolated  
350 mAbs in SARS-CoV-2, and bind an epitope on the 'neck'<sup>17</sup>. IGHV53/66 thus forms a major public  
351 antibody response and it is no surprise that the virus has evolved to escape this response.  
352 Mutations found in previous VoC lead to loss of function of many IGHV53/66 mAbs, but this  
353 antibody class has proved to be very adaptable to accommodate change<sup>20</sup> and it would seem



354 likely that somatic mutation will allow the response to adapt to the N460K mutation following  
355 BA.2.75 infection.

356

357 Interestingly, BA.2.75 has also acquired the R493Q reversion (Q493R was acquired in BA.1 and  
358 present in all other Omicron sublineages except BA.4/5). Here we show that BA.2.75 RBD is able  
359 to bind ACE2 with 9-fold higher affinity than BA.2 and more tightly than BA.4/5<sup>12,15</sup>. BA.2.75 has  
360 the highest ACE2 affinity among all SARS-CoV-2 variants we have measured to date and we show  
361 that this is partly attributable to the R493Q mutation. Although we have been unable to express  
362 BA.2+N460K RBD, previous studies show N460K can enhance RBD binding for ACE2, an effect  
363 similar in magnitude to that seen with the N501Y mutation described initially in Alpha<sup>11</sup>, thus,  
364 N460K probably both enhances antibody escape and increases receptor binding affinity.

365

366 There is likely a fine interplay between antibody escape and ACE2 receptor affinity; Alpha (N501Y)  
367 evolved early during the pandemic, when the background population SARS-CoV-2 exposure was  
368 relatively low. Although neutralization titres against Alpha were modestly reduced compared to  
369 ancestral strains<sup>29</sup>, it is likely that the major driver for the evolution of Alpha N501Y was an  
370 increase in ACE2 affinity, giving the virus a transmission advantage<sup>30</sup>. Currently, population  
371 exposure to SARS-CoV-2 by either natural infection or vaccination is high, leading to the dual  
372 pressure of increased ACE2 affinity and antibody evasion. For the R493Q reversion, the balance  
373 between a reduction in antibody escape but increased ACE2 affinity may have tipped to allow  
374 BA.2.75 to more effectively transmit in certain populations. Other factors such as spike stability,

375 replication time and reduced TMPRSS2 dependence also influence the success of SARS-CoV-2  
376 variants<sup>30-33</sup>.

377

378 BA.2.75 has become the dominant SARS-CoV-2 strain in India and it will soon become clear  
379 whether BA.2.75 is able to outcompete BA.4/5 to become the globally dominant strain, or  
380 whether it will remain regionally localised, as was the case for Beta and Gamma. If the latter, it  
381 may reflect the different background immunity of the population. India, where BA.2.75 seems to  
382 have originated, has a very high background of Delta infection. Using neutralization assays we  
383 show Delta infection in isolation, provides no protection (no neutralization) against BA.2.75. In  
384 other countries where vaccination programmes are more advanced, together with the high level  
385 of Omicron immunity, there may be sufficient protection to check BA.2.75.

386

387 Very recently a number of new variants have been emerging based upon BA.5 or BA.2.75,  
388 including BA.2.3.20, BA.2.75.2, BA.2.10.4, BJ.1 amongst others, these variants have picked up a  
389 host of additional mutations in the RBD, with evidence of co-evolution of a number of residues  
390 and appear to be selected to increase escape from Omicron neutralizing serum  
391 (<https://www.biorxiv.org/content/10.1101/2022.09.15.507787v3>).

392

393 In summary, we show the mutations in BA.2.75 lead to a reduction in neutralization titres of  
394 vaccine serum compared to BA.2. Individual BA.2.75 mutations can cause greater reduction in

395 neutralization titres compared to the full BA.2.75 S sequence, but these are balanced by the  
396 R393Q reversion mutation, which may have been selected to increase affinity to ACE2 and  
397 increase the transmissibility of BA.2.75. It seems inevitable that further evolution of the Omicron  
398 lineage will occur and there are likely many possible trade-offs between antibody escape and  
399 ACE2 affinity, that can and will be made, leading to successive waves of infection.

400

#### 401 **Limitations of the study**

402 Limitations of this study are that the *in vitro* neutralization assays we used do not probe the full  
403 function of the antibody response as they do not measure the effects of complement or antibody  
404 dependent cell mediated cytotoxicity which operate *in vivo*. In addition, as live BA.2.75 virus was  
405 not available in our laboratory we relied on lentiviral pseudoneutralization assays for  
406 characterization. Furthermore, they do not take account of T cell responses, which have been  
407 shown to be more resilient to the mutations expressed by VoC.

408

#### 409 **Figure legends**

410 **Figure 1. Sequence changes in BA.2.75 compared to other Omicron sub-lineages.** (A) Sequence  
411 alignments of BA.2.75 together with Omicron sublineages Omicron BA.1, BA.1.1, BA.2, BA.3 and  
412 BA.4/5 boundaries of the NTD and RBD are marked. (B) Surface representation of mutated  
413 residues in BA.2.75 RBD in comparison to BA.2 RBD. Position of BA.2 RBD mutations (grey surface

414 with the ACE2 footprint in dark green) are shown and residues mutated in BA.2.75 are shown in  
415 orange and labelled.

416

417 **Figure 2. Pseudoviral neutralization assays of BA.2.75 by vaccine and BA.1 and BA.2 immune**  
418 **serum.** IC50 values for the indicated viruses using serum obtained from vaccinees 28 days  
419 following their third dose of vaccine (A) Pfizer BNT162b2 (n=22), (B) AstraZeneca AZD AZD1222  
420 (n=41). (C-E) Serum from volunteers suffering vaccine breakthrough BA.1 (n=16), BA.2 (n=23) or  
421 BA.4/5 (n=11) infections. (F) IC50 values for single RBD point mutations inserted into the BA.2  
422 pseudovirus using Pfizer BNT162b2 serum (n=22) Geometric mean titres are shown above each  
423 column. The Wilcoxon matched-pairs signed rank test was used for the analysis and two-tailed P  
424 values were calculated. See also Table S3.

425

426 **Figure 3 ACE2/RBD affinity.** SPR sensorgrams showing ACE2 binding of BA.2.75 RBD using ACE2-  
427 Fc (A) or biotinylated ACE2 as ligand (B) in comparison to binding to the RBD of BA.2 (C), BA.4/5  
428 (D), Alpha (E) and BA.2+R493Q (F). The data for BA.2, BA.4/5 and Alpha have been reported  
429 previously in references 12,15 and 20 respectively.

430

431 **Figure 4 The Structure of BA.2.75 RBD/ACE2 complex.** (A) Front and back views of the overall  
432 structure of the BA.2.75 RBD/ACE2 complex. ACE2 is shown as green ribbons and the RBD as  
433 surface with mutations common to BA.2 highlighted in magenta and different in orange. (B)

434 BA.2.75 RBD (grey) and ACE2 (green) interface compared with that of BA.2 and ACE2 (both in  
435 salmon). Closeups show interactions of Q496R and Q493 (R493 in BA.2) with ACE2. See also Table  
436 S5.

437

438 **Figure 5. Pseudoviral neutralization assays against monoclonal antibodies.** (A) Neutralization  
439 curves for a panel of 28 mAb made from samples taken from vaccinees infected with BA.1.  
440 Titration curves for BA.2.75 are compared with Victoria, BA.1, BA.1.1, BA.2 and BA.4/5. IC50 titres  
441 are shown in Table S1A. (B) Pseudoviral neutralization assays with mAbs developed for human  
442 use. IC50 titres are shown in Table S1B. Data for Victoria, BA.1, BA.1.1 and BA.2 and BA.4/5 are  
443 used for comparison and taken from<sup>12</sup>. See also Figure S1. All assays have been done at least  
444 twice.

445

446 **Figure 6 Interactions between mAbs and BA.2.75 mutation sites.** (A) Front and back views of the  
447 binding modes of Omi-3 (PDB, 7ZF3) and Omi-18 (PDB, 7ZFC) complexed with Omicron BA.1 RBD  
448 by overlapping the RBD. The RBD is shown as grey surface representation with mutations  
449 common to both BA.2 and BA.2.75 coloured in magenta, and the four mutations different  
450 between the two in cyan. Vhs and Vls are shown as ribbons and coloured in red and blue for Omi-  
451 3, and light blue and salmon for Omi-18, respectively. (B) Interactions between N460 of the RBD  
452 and CDR-H2 of the Fabs. (C) Contacts between R493 of the RBD and CDR-H3 of the Fabs. In (B)  
453 and (C) The RBD associated with Omi-3 is in grey and Omi-18 in cyan, and the colours of the Fabs  
454 are as in (A). (D) AZD1061 bound with the ancestral SARS-CoV-2 RBD (PDB, 7L7E) and (E) contacts

455 between G446 of the RBD and CDR-L2 of the Fab. (E) AZD8895 bound with the ancestral SARS-  
456 CoV-2 spike RBD (PDB, 7L7E) and (F) contacts between Q493 of the RBD and CDR-H2 of the Fab.  
457 In (D)-(F), RBD is drawn and coloured as in (A), HC is in red and LC in blue.

458

459 **Figure 7 Antigenic mapping.** (A) Orthogonal views of the antigenic map showing BA.2.75 in the  
460 context of the positions of previous VoC and BA.1, BA.1.1, BA.1 and BA.2, calculated from  
461 pseudovirus neutralisation data. Distance between two positions is proportional to the reduction  
462 in neutralisation titre when one of the corresponding strains is challenged with serum derived by  
463 infection by the other. No scale is provided since the figures are projections of a three-  
464 dimensional distribution, however the variation can be calibrated by comparison with (i) BA.1 to  
465 BA.2 which is 2.93x reduced and (ii) BA.2 to BA.4/5 which is 3.03x reduced. (B) As (A) but including  
466 only Omicron sublineages and early pandemic viruses to allow more accurate projection of this  
467 subset into three-dimensions. Note that responses of these viruses against all sera were included  
468 in the calculations. See also Table S1.

469

#### 470 **Acknowledgements**

471 This work was supported by the Chinese Academy of Medical Sciences (CAMS) Innovation Fund  
472 for Medical Science (CIFMS), China (grant number: 2018-I2M-2-002) to D.I.S. and G.R.S. We are  
473 also grateful for support from Schmidt Futures, the Red Avenue Foundation and the Oak  
474 Foundation. G.R.S. was supported by Wellcome. H.M.E.D., and J.R. are supported by Wellcome  
475 (101122/Z/13/Z), D.I.S. and E.E.F. by the UKRI MRC (MR/N00065X/1). D.I.S. and G.R.S. are Jenner

476 Investigators. This is a contribution from the UK Instruct-ERIC Centre. AJM is an NIHR-supported  
477 Academic Clinical Lecturer. The convalescent sampling was supported by the Medical Research  
478 Council [grant MC\_PC\_19059] (awarded to the ISARIC-4C consortium) (with a full contributor list  
479 available at <https://isaric4c.net/about/authors/>) and the National Institutes for Health and  
480 Oxford Biomedical Research Centre and an Oxfordshire Health Services Research Committee  
481 grant to AJM. OPTIC Consortium: Christopher Conlon, Alexandra Deeks, John Frater, Lisa Frending,  
482 Siobhan Gardiner, Anni Jämsén, Katie Jeffery, Tom Malone, Eloise Phillips, Lucy Rothwell, Lizzie  
483 Stafford. The Wellcome Centre for Human Genetics is supported by the Wellcome Trust (grant  
484 090532/Z/09/Z). The computational aspects of this research were supported by the Wellcome  
485 Trust Core Award Grant Number 203141/Z/16/Z and the NIHR Oxford BRC.

486 The Oxford Vaccine work was supported by UK Research and Innovation, Coalition for Epidemic  
487 Preparedness Innovations, National Institute for Health Research (NIHR), NIHR Oxford Biomedical  
488 Research Centre, Thames Valley and South Midland's NIHR Clinical Research Network. We thank  
489 the Oxford Protective T-cell Immunology for COVID-19 (OPTIC) Clinical team for participant  
490 sample collection and the Oxford Immunology Network Covid-19 Response T cell Consortium for  
491 laboratory support. We acknowledge the rapid sharing of Victoria, B.1.1.7 and B.1.351 which was  
492 isolated by scientists within the National Infection Service at PHE Porton Down, and the B.1.617.2  
493 virus was kindly provided Wendy Barclay and Thushan de Silva. We thank The Secretariat of  
494 National Surveillance, Ministry of Health Brazil for assistance in obtaining P.1 samples. This work  
495 was supported by the UK Department of Health and Social Care as part of the PITCH (Protective  
496 Immunity from T cells to Covid-19 in Health workers) Consortium, the UK Coronavirus  
497 Immunology Consortium (UK-CIC) and the Huo Family Foundation. We acknowledge Diamond

498 Light Source for time on Beamline I03 under Proposal Ib27009 for COVID-19 Rapid Access. We  
499 thank the staff of the MRC Human Immunology Unit for access to their Biacore Facility. EB and PK  
500 are NIHR Senior Investigators and PK is funded by WT222426/Z/21/Z and NIH (U19 I082360). SJD  
501 is funded by an NIHR Global Research Professorship (NIHR300791). DS is an NIHR Academic  
502 Clinical Fellow. The Sheffield Teaching Hospitals Observational Study of Patients with Pulmonary  
503 Hypertension, Cardiovascular and other Respiratory Diseases (STH-ObS) was supported by the  
504 British Heart Foundation ([PG/11/116/29288](#)). The STH-ObS Chief Investigator Allan Lawrie is  
505 supported by a British Heart Foundation Senior Basic Science Research fellowship  
506 ([FS/18/52/33808](#)). We gratefully acknowledge financial support from the UK Department of  
507 Health via the Sheffield NIHR Clinical Research Facility award to the Sheffield Teaching Hospitals  
508 Foundation NHS Trust. The views expressed in this article are those of the authors and not  
509 necessarily those of the National Health Service (NHS), the Department of Health and Social Care  
510 (DHSC), the National Institutes for Health Research (NIHR), the Medical Research Council (MRC)  
511 or Public Health, England.

512

### 513 **Author Information**

514 These authors contributed equally: J.H., A.D-G. and C.L.

515

### 516 **Contributions**



517 J.H. performed interaction affinity analyses. D.Z. performed antibody competition analyses. D.Z.,  
518 J.H., J.R., N.G.P., M.A.W., and D.R.H. prepared the crystals and enabled and performed X-ray data  
519 collection. J.R., E.E.F., H.M.E.D. and D.I.S. analyzed the structural results. G.R.S., J.H., J.M., P.S.,  
520 D.Z., R.N., A.T., A.D-G., M.S., R.D. and C.L. prepared the RBDs, ACE2, and antibodies, and C.L., and  
521 P.S. performed neutralization assays. P.S. isolated all Omicron variants. D.C., H.W., B.C., and N.T.  
522 provided materials. H.M.G. wrote mabscape and performed mapping and cluster analysis,  
523 including sequence and antigenic space analyses. A.J.M., D.S., T.G.R., A.A., S.B., S.A., S.A.J., P.K.,  
524 E.B. S.J.D., A.J.P., T.L., and P.G. assisted with patient samples and vaccine trials. E.B., S.J.D., and  
525 P.K. conceived the study of vaccinated healthcare workers and oversaw the OPTIC Healthcare  
526 Worker study and sample collection/processing. T.I.d-S, M.P., T.A.H.N and H.H. assisted with  
527 healthcare worker recruitment and sample collection in the Sheffield STHObs study. G.R.S., and  
528 D.I.S. conceived the study. G.R.S., D.I.S. and J.H. wrote the initial manuscript draft with other  
529 authors providing editorial comments. All authors read and approved the manuscript.

530

### 531 **Competing Financial Interests**

532 G.R.S. sits on the GSK Vaccines Scientific Advisory Board, consults for Astra Zeneca and is a  
533 founder member of RQ Biotechnology. Oxford University holds intellectual property related to  
534 the Oxford-Astra Zeneca vaccine and SARS-CoV-2 mAb discovered in G.R.S.'s laboratory. A.J.P. is  
535 Chair of UK Dept. Health and Social Care's (DHSC) Joint Committee on Vaccination &  
536 Immunisation (JCVI) but does not participate in the JCVI COVID-19 committee, and is a member  
537 of the WHO's SAGE. The views expressed in this article do not necessarily represent the views of  
538 DHSC, JCVI, or WHO. The University of Oxford has entered into a partnership with AstraZeneca

539 on coronavirus vaccine development. T.L. is named as an inventor on a patent application  
540 covering this SARS-CoV-2 vaccine and was a consultant to Vaccitech for an unrelated project  
541 whilst the study was conducted. S.J.D. is a Scientific Advisor to the Scottish Parliament on COVID-  
542 19.

543

#### 544 **STAR Methods**

545

#### 546 **DATA AND CODE AVAILABILITY**

547 • *Data availability.* The coordinates and structure factors of the crystallographic complex are  
548 available from the PDB with accession code 8ASY.

549

550 • *Code availability.* This paper does not report original code.

551

552 • Reagents generated in this study are available from the lead contact with a completed  
553 Materials Transfer Agreement. Any additional information required to reanalyze the  
554 data reported in this paper is available from the lead contact upon request.

555

556 • Additional Supplemental Items are available from Mendeley Data  
557 at <http://dx.doi.org/10.17632/4sj8trtw62.1>

558

559 **EXPERIMENTAL MODEL AND SUBJECT DETAILS**560 *Bacterial Strains and Cell Culture*

561 Vero (ATCC CCL-81) and VeroE6/TMPRSS2 cells were cultured at 37 °C in Dulbecco's Modified  
562 Eagle medium (DMEM) high glucose (Sigma-Aldrich) supplemented with 10% fetal bovine serum  
563 (FBS), 2 mM GlutaMAX (Gibco, 35050061) and 100 U/ml of penicillin–streptomycin. Human mAbs  
564 were expressed in HEK293T cells cultured in UltraDOMA PF Protein-free Medium (Cat# 12-727F,  
565 LONZA) at 37 °C with 5% CO<sub>2</sub>. HEK293T (ATCC CRL-11268) cells were cultured in DMEM high  
566 glucose (Sigma-Aldrich) supplemented with 10% FBS, 1% 100X Mem Neaa (Gibco) and 1% 100X L-  
567 Glutamine (Gibco) at 37 °C with 5% CO<sub>2</sub>. To express RBD, RBD variants and ACE2, HEK293T cells  
568 were cultured in DMEM high glucose (Sigma) supplemented with 2% FBS, 1% 100X Mem Neaa  
569 and 1% 100X L-Glutamine at 37 °C for transfection. Omicron RBD and human mAbs were also  
570 expressed in HEK293T (ATCC CRL-11268) cells cultured in FreeStyle 293 Expression Medium  
571 (ThermoFisher, 12338018) at 37 °C with 5% CO<sub>2</sub>. *E.coli DH5α* bacteria were used for  
572 transformation and large-scale preparation of plasmids. A single colony was picked and cultured  
573 in LB broth at 37 °C at 200 rpm in a shaker overnight.

574

575 *Plasma from early pandemic and Alpha cases*

576 Participants from the first wave of SARS-CoV2 in the U.K. and those sequence confirmed with  
577 B.1.1.7 lineage in December 2020 and February 2021 were recruited through three studies: Sepsis  
578 Immunomics [Oxford REC C, reference:19/SC/0296], ISARIC/WHO Clinical Characterisation

579 Protocol for Severe Emerging Infections [Oxford REC C, reference 13/SC/0149] and the Gastro-  
580 intestinal illness in Oxford: COVID sub study [Sheffield REC, reference: 16/YH/0247]. Diagnosis  
581 was confirmed through reporting of symptoms consistent with COVID-19 and a test positive for  
582 SARS-CoV-2 using reverse transcriptase polymerase chain reaction (RT-PCR) from an upper  
583 respiratory tract (nose/throat) swab tested in accredited laboratories. A blood sample was taken  
584 following consent at least 14 days after symptom onset. Clinical information including severity of  
585 disease (mild, severe or critical infection according to recommendations from the World Health  
586 Organisation) and times between symptom onset and sampling and age of participant was  
587 captured for all individuals at the time of sampling. Following heat inactivation of plasma/serum  
588 samples they were aliquoted so that no more than 3 freeze thaw cycles were performed for data  
589 generation. For subject details see Table S3.

590

591 Sera from BA.4/5 infected cases, study subjects

592 Following informed consent, individuals with omicron BA.4 or BA.5 were co-enrolled into one or more of  
593 the following three studies: the ISARIC/WHO Clinical Characterisation Protocol for Severe Emerging  
594 Infections [Oxford REC C, reference 13/SC/0149], the “Innate and adaptive immunity against SARS-CoV-2  
595 in healthcare worker family and household members” protocol (approved by the University of Oxford  
596 Central University Research Ethics Committee), or the Gastro-intestinal illness in Oxford: COVID sub study  
597 [Sheffield REC, reference: 16/YH/0247]. Diagnosis was confirmed through reporting of symptoms  
598 consistent with COVID-19, hospital presentation, and a test positive for SARS-CoV-2 using reverse  
599 transcriptase polymerase chain reaction (RT-PCR) from an upper respiratory tract (nose/throat) swab  
600 tested in accredited laboratories and lineage sequence confirmed through national reference laboratories

601 in the United Kingdom. A blood sample was taken following consent at least 14 days after PCR test  
602 confirmation. Clinical information including severity of disease (mild, severe or critical infection according  
603 to recommendations from the World Health Organisation) and times between symptom onset and  
604 sampling and age of participant was captured for all individuals at the time of sampling. For subject  
605 details see Table S3.

606

607 *Sera from Beta, Gamma and Delta infected cases*

608 Beta and Delta samples from UK infected cases were collected under the “Innate and adaptive  
609 immunity against SARS-CoV-2 in healthcare worker family and household members” protocol  
610 affiliated to the Gastro-intestinal illness in Oxford: COVID sub study discussed above and  
611 approved by the University of Oxford Central University Research Ethics Committee. All  
612 individuals had sequence confirmed Beta/Delta infection or PCR-confirmed symptomatic disease  
613 occurring whilst in isolation and in direct contact with Beta/Delta sequence-confirmed cases.  
614 Additional Beta infected serum (sequence confirmed) was obtained from South Africa. At the time  
615 of swab collection patients signed an informed consent to consent for the collection of data and  
616 serial blood samples. The study was approved by the Human Research Ethics Committee of the  
617 University of the Witwatersrand (reference number 200313) and conducted in accordance with  
618 Good Clinical Practice guidelines. Gamma samples were provided by the International Reference  
619 Laboratory for Coronavirus at FIOCRUZ (WHO) as part of the national surveillance for coronavirus  
620 and had the approval of the FIOCRUZ ethical committee (CEP 4.128.241) to continuously receive  
621 and analyse samples of COVID-19 suspected cases for virological surveillance. Clinical samples

622 were shared with Oxford University, UK under the MTA IOC FIOCRUZ 21-02. For subject details  
623 see Table S3.

624

625

626 *Sera from BA.1 infected cases, study subjects*

627 Following informed consent, individuals with omicron BA.1 were co-enrolled into the ISARIC/WHO Clinical  
628 Characterisation Protocol for Severe Emerging Infections [Oxford REC C, reference 13/SC/0149] and the  
629 “Innate and adaptive immunity against SARS-CoV-2 in healthcare worker family and household members”  
630 protocol affiliated to the Gastro-intestinal illness in Oxford: COVID sub study [Sheffield REC, reference:  
631 16/YH/0247] further approved by the University of Oxford Central University Research Ethics Committee.  
632 Diagnosis was confirmed through reporting of symptoms consistent with COVID-19 or a positive contact  
633 of a known Omicron case, and a test positive for SARS-CoV-2 using reverse transcriptase polymerase chain  
634 reaction (RT-PCR) from an upper respiratory tract (nose/throat) swab tested in accredited laboratories and  
635 lineage sequence confirmed through national reference laboratories. A blood sample was taken following  
636 consent at least 10 days after PCR test confirmation. Clinical information including severity of disease (mild,  
637 severe or critical infection according to recommendations from the World Health Organisation) and times  
638 between symptom onset and sampling and age of participant was captured for all individuals at the time  
639 of sampling. For subject details see Table S3.

640

641 *Sera from BA.2 infected cases, study subjects*

642 Following informed consent, healthcare workers with BA.2 infection were co-enrolled under the Sheffield  
643 Biobank study (STHObs) (18/YH/0441). All individuals had PCR-confirmed symptomatic disease and

644 sequence confirmed BA.2 infection through national UKHSA sequencing data. A blood sample was taken  
645 following consent at least 12 days after PCR test confirmation. Clinical information including vaccination  
646 history, times between symptom onset and sampling and age of participant was captured for all individuals  
647 at the time of sampling. For subject details see Table S3.

648

#### 649 *Sera from Pfizer vaccinees*

650 Pfizer vaccine serum was obtained from volunteers who had received three doses of the  
651 BNT162b2 vaccine. Vaccinees were Health Care Workers, based at Oxford University Hospitals  
652 NHS Foundation Trust, not known to have prior infection with SARS-CoV-2 and were enrolled in  
653 the OPTIC Study as part of the Oxford Translational Gastrointestinal Unit GI Biobank Study  
654 16/YH/0247 [research ethics committee (REC) at Yorkshire & The Humber – Sheffield] which has  
655 been amended for this purpose on 8 June 2020. The study was conducted according to the  
656 principles of the Declaration of Helsinki (2008) and the International Conference on  
657 Harmonization (ICH) Good Clinical Practice (GCP) guidelines. Written informed consent was  
658 obtained for all participants enrolled in the study. Participants were sampled approximately 28  
659 days (range 25-56) after receiving a third “booster dose of BNT162B2 vaccine. The mean age of  
660 vaccinees was 37 years (range 22-66), 21 male and 35 female.

661

#### 662 *AstraZeneca-Oxford vaccine study procedures and sample processing*

663 Full details of the randomized controlled trial of ChAdOx1 nCoV-19 (AZD1222), were previously  
664 published (PMID: 33220855/PMID: 32702298). These studies were registered at ISRCTN

665 (15281137 and 89951424) and ClinicalTrials.gov (NCT04324606 and NCT04400838). Written  
666 informed consent was obtained from all participants, and the trial is being done in accordance  
667 with the principles of the Declaration of Helsinki and Good Clinical Practice. The studies were  
668 sponsored by the University of Oxford (Oxford, UK) and approval obtained from a national ethics  
669 committee (South Central Berkshire Research Ethics Committee, reference 20/SC/0145 and  
670 20/SC/0179) and a regulatory agency in the United Kingdom (the Medicines and Healthcare  
671 Products Regulatory Agency). An independent DSMB reviewed all interim safety reports. A copy  
672 of the protocols was included in previous publications<sup>34</sup>. Data from vaccinated volunteers who  
673 received three vaccinations are included in this study. Blood samples were collected and serum  
674 separated approximately 28 days (range 26-34 days) following the third dose. For subject details  
675 see column 'AZ V3+28' in Table S3.

676

## 677 **Method Details**

### 678 *Pseudovirus plasmid construction and lentiviral particles production*

679 Pseudotyped lentivirus expressing SARS-CoV-2 S proteins from ancestral strain (Victoria, S247R),  
680 BA.1, BA.1.1, BA.2 and BA.4/5 were constructed as described previously<sup>12,14,20,35</sup>. We applied the  
681 same method to construct BA.2.12.1, and BA.2.75, by adding more mutations into the BA.2  
682 construct. To generate BA.2.75, we added K147E, W152R, F157L, I210V, G275S, G446S and  
683 N460K into BA.2 backbone, also changed 339D in BA.2 S into 339H, and reversed 493R in BA.2 to  
684 493Q as in the ancestral strain. To test single mutation impact, we introduced D339H, G446S,  
685 N460K and R493Q individually into BA.2 backbone. The resulting pcDNA3.1 plasmid carrying S



686 gene was used for generating pseudoviral particles together with the lentiviral packaging vector  
687 and transfer vector encoding luciferase reporter. All the constructs were sequence confirmed.

688

#### 689 *Pseudoviral neutralization test*

690 The pseudoviral neutralization test has been described previously<sup>14</sup>. Briefly, the neutralizing  
691 activity of potent monoclonal antibodies generated from donors who had recovered from BA.1  
692 infection were tested against Victoria, BA.1, BA.1.1, BA.2, BA.3, BA.4/5, BA.2.75 and BA.2+N460K.  
693 Four-fold serial diluted mAbs were incubated with pseudoviral particles at 37°C, 5% CO<sub>2</sub> for 1 hr.  
694 Stable HEK293T/17 cells expressing human ACE2 were then added to the mixture at  $1.5 \times 10^4$   
695 cells/well. 48 hr post infection, culture supernatants were removed and 50 µL of 1:2 Bright-Glo  
696 TM Luciferase assay system (Promega, USA) in 1 × PBS was added to each well. The reaction was  
697 incubated at room temperature for 5 mins and firefly luciferase activity was measured using  
698 CLARIOstar® (BMG Labtech, Ortenberg, Germany). The percentage neutralization was calculated  
699 relative to the control. Probit analysis was used to estimate the dilution that inhibited half  
700 maximum pseudotyped lentivirus infection (PVNT50).

701 To determine the neutralizing activity of convalescent plasma/serum samples or vaccine sera, 3-  
702 fold serial dilutions of each samples were incubated with pseudoviral particles for 1 hr and the  
703 same strategy as mAb was applied.

704

#### 705 *Cloning of RBDs*

706 To generate the BA.2.75 RBD construct, site-directed PCR mutagenesis was performed using the  
707 BA.2 Spike construct as the template<sup>20</sup>, with the introduction of D339H, G446S, N460K and R493Q  
708 mutations using primers listed in Table S4; the gene fragment was amplified with D339H\_pNeoF  
709 and RBD333\_BAP\_R (Table S4), and cloned into the pOPINTTGneo-BAP vector<sup>36</sup>. To generate the  
710 BA.2+R493Q RBD construct, site-directed PCR mutagenesis was performed using the BA.2 Spike  
711 construct as the template, with the introduction of R493Q mutation using primers listed in Table  
712 S4; the gene fragment was amplified with pNeoRBD333Omi\_F and RBD333\_BAP\_R, and cloned  
713 into the pNeo vector<sup>13</sup>. Cloning was performed using the ClonExpress II One Step Cloning Kit  
714 (Vazyme). The Constructs were verified by Sanger sequencing after plasmid isolation using  
715 QIAGEN Miniprep kit (QIAGEN).

716

#### 717 *Production of RBDs*

718 Plasmids encoding RBDs were transfected into Expi293F™ Cells (ThermoFisher) by PEI, cultured  
719 in FreeStyle™ 293 Expression Medium (ThermoFisher) at 37 °C for 1 day followed by 30 °C for 3  
720 days with 8% CO<sub>2</sub>. To express biotinylated RBDs, the RBD-BAP plasmid was co-transfected with  
721 pDisplay-BirA-ER (Addgene plasmid 20856; coding for an ER-localized biotin ligase), in the  
722 presence of 0.8 mM D-biotin (Sigma-Aldrich). The conditioned medium was diluted 1:2 into  
723 binding buffer (50 mM sodium phosphate, 500 mM sodium chloride, pH 8.0). RBDs were purified  
724 with a 5 mL HisTrap nickel column (GE Healthcare) through His-tag binding, followed by a  
725 Superdex 75 10/300 GL gel filtration column (GE Healthcare) in 10 mM HEPES and 150 mM  
726 sodium chloride.

727

728 *Surface Plasmon Resonance*

729 Surface plasmon resonance experiments were performed using a Biacore T200 (GE Healthcare).

730 All assays were performed with running buffer of HBS-EP (Cytiva) at 25 °C.

731

732 To determine the binding kinetics between BA.2.75 or BA.2+R493Q RBD and ACE2, a Protein A  
733 sensor chip (Cytiva) was used. ACE2-Fc was immobilised onto the sample flow cell of the sensor  
734 chip. The reference flow cell was left blank. RBD was injected over the two flow cells at a range  
735 of five concentrations prepared by serial two-fold dilutions, at a flow rate of 30  $\mu\text{l min}^{-1}$  using a  
736 single-cycle kinetics programme. Running buffer was also injected using the same programme  
737 for background subtraction. All data were fitted to a 1:1 binding model using Biacore T200  
738 Evaluation Software 3.1.

739

740 To confirm the binding kinetics between the BA.2.75 RBD and ACE2, a Biotin CAPture Kit (Cytiva)  
741 was used. Biotinylated ACE2 (bio-ACE2) was immobilised onto the sample flow cell of the sensor  
742 chip. The reference flow cell was left blank. The BA.2.75 RBD was injected over the two flow cells  
743 at a range of five concentrations prepared by serial two-fold dilutions, at a flow rate of 30  $\mu\text{l min}^{-1}$   
744 using a single-cycle kinetics programme. Running buffer was also injected using the same  
745 programme for background subtraction. All data were fitted to a 1:1 binding model using Biacore  
746 T200 Evaluation Software 3.1.

747

748 To determine the binding kinetics between the BA.2.75 or BA.2 RBD and mAbs, a Biotin CAPture  
749 Kit (Cytiva) was used. Biotinylated RBD was immobilised onto the sample flow cell of the sensor  
750 chip. The reference flow cell was left blank. The Fab of Omi-18 or Omi-32 was injected over the  
751 two flow cells at a range of five concentrations prepared by serial two-fold dilutions, at a flow  
752 rate of  $30 \mu\text{l min}^{-1}$  using a single-cycle kinetics programme. For the binding of Omi-20 for bio-  
753 BA.2 RBD, the Fab of Omi-20 was injected over the two flow cells at a range of five concentrations  
754 prepared by serial two-fold dilutions, at a flow rate of  $30 \mu\text{l min}^{-1}$  using a single-cycle kinetics  
755 programme. For the binding of Omi-20 for bio-BA.2.75 RBD, the Fab of Omi-20 was injected over  
756 the two flow cells at a range of eight concentrations prepared by serial twofold dilutions, at a  
757 flow rate of  $30 \mu\text{l min}^{-1}$ . Running buffer was also injected using the same programme for  
758 background subtraction. All data were fitted to a 1:1 binding model using Biacore T200 Evaluation  
759 Software 3.1.

760

761 To compare the binding profiles between BA.2 and BA.2.75 RBD for mAb Omi-29, a Biotin  
762 CAPture Kit (Cytiva) was used. Biotinylated BA.2 and BA.2.75 RBD was immobilised onto the  
763 sample flow cell of the sensor chip to a similar level ( $\sim 110$  RU). The reference flow cell was left  
764 blank. A single injection of mAb Fab was performed over the two flow cells at  $1 \mu\text{M}$ , at a flow rate  
765 of  $30 \mu\text{l min}^{-1}$ . Running buffer was also injected using the same programme for background  
766 subtraction. The sensorgrams were plotted using Prism9 (GraphPad).

767

768 To compare the binding profiles between BA.2 and BA.2.75 RBD for mAb Omi-36, a sensor chip  
769 Protein A (Cytiva) was used. mAb Omi-36 in the IgG form was immobilised onto the sample flow  
770 cell of the sensor chip. The reference flow cell was left blank. A single injection of RBD was  
771 performed over the two flow cells at 200 nM, at a flow rate of 30  $\mu\text{l min}^{-1}$ . Running buffer was  
772 also injected using the same programme for background subtraction. The sensorgrams were  
773 plotted using Prism9 (GraphPad).

774

#### 775 *IgG mAbs and Fabs production*

776 AstraZeneca and Regeneron antibodies were provided by AstraZeneca, Vir, Lilly and Adagio  
777 antibodies were provided by Adagio, LY-CoV1404 was provided by LifeArc. For the in-house  
778 antibodies, heavy and light chains of the indicated antibodies were transiently transfected into  
779 293T cells and antibody purified from supernatant on protein A as previously described<sup>20</sup>. Fabs  
780 were digested from purified IgGs with papain using a Pierce Fab Preparation Kit (Thermo Fisher),  
781 following the manufacturer's protocol.

782

#### 783 *Crystallization, X-ray data collection and structure determination*

784 Purified BA.2.75 RBD was deglycosylated with Endoglycosidase H1 and mixed with ACE2 in a 1:1  
785 molar ratio, with a final concentration of 13.0 mg ml<sup>-1</sup>. Initial screening of crystals was set up in  
786 Crystalquick 96-well X plates (Greiner Bio-One) with a Cartesian Robot using the nanoliter sitting-  
787 drop vapor-diffusion method, with 100 nL of protein plus 100 nL of reservoir in each drop, as

788 previously described<sup>37</sup>. Crystals of BA.2.75 RBD-ACE2 complex were formed in Hampton Research  
789 PEGRx condition 2-25, containing 0.1% (w/v) n-Octyl-b-D-glucoside, 0.1 M Sodium citrate tribasic  
790 dihydrate pH 5.5 and 22% (w/v) PEG 3350. Crystals were mounted in loops and dipped in solution  
791 containing 25% glycerol and 75% mother liquor for a second before frozen in liquid nitrogen.  
792 Diffraction data were collected at 100 K at beamline I03 of Diamond Light Source, UK, using the  
793 automated queue system that allows unattended automated data collection  
794 ([https://www.diamond.ac.uk/Instruments/Mx/I03/I03-Manual/Unattended-Data-](https://www.diamond.ac.uk/Instruments/Mx/I03/I03-Manual/Unattended-Data-Collections.html)  
795 [Collections.html](https://www.diamond.ac.uk/Instruments/Mx/I03/I03-Manual/Unattended-Data-Collections.html)). The best crystal diffracted to 2.85 Å resolution. 3600 diffraction images of 0.1°  
796 each were collected and automatically processed with Xia2-dials<sup>38,39</sup>. The structure was  
797 determined by rigid body refinement using the model of BA.2 RBD/ACE2 complex (PDB, 7ZF7)<sup>20</sup>  
798 of which the unit cell is isomorphous to the current crystal. Model rebuilding is done with COOT<sup>40</sup>  
799 and refinement with Phenix<sup>41</sup>.

800

801 Data collection and structure refinement statistics are given in **Table S5**. Structural comparisons  
802 used SHP<sup>42</sup> and figures were prepared with PyMOL (The PyMOL Molecular Graphics System,  
803 Version 1.2r3pre, Schrödinger, LLC).

804

#### 805 *Antigenic mapping*

806 Antigenic mapping of omicron was carried out using a previously described<sup>12</sup>. In short,  
807 coronavirus variants were assigned three-dimensional coordinates whereby the distance  
808 between two points indicates the base drop in neutralization titre. Each serum was assigned a

809 strength parameter which provided a scalar offset to the logarithm of the neutralization titre.  
810 These parameters were refined to match predicted neutralization titres to observed values by  
811 taking an average of superimposed positions from 30 separate runs. The three-dimensional  
812 positions of the variants of concern: Victoria, Alpha, Beta, Gamma, Delta and Omicron were  
813 plotted for display.

814

#### 815 *Quantification and statistical analysis*

816 Statistical analyses are reported in the results and figure legends. Neutralization was measured  
817 on pseudovirus. The percentage reduction was calculated and IC<sub>50</sub> determined using the probit  
818 program from the SPSS package. The Wilcoxon matched-pairs signed rank test was used for the  
819 analysis and two-tailed P values were calculated on geometric mean values.

820

821 **Video S1.** Three-dimensional antigenic map of all VoC. Related to Figure 7.

822

823 **Video S2.** Three-dimensional antigenic map of early pandemic viruses and Omicron variants.  
824 Related to Figure 7.

825

#### 826 **References**

- 827 1. Robson, F., Khan, K.S., Le, T.K., Paris, C., Demirbag, S., Barfuss, P., Rocchi, P., and Ng, W.L. (2020).  
828 Coronavirus RNA Proofreading: Molecular Basis and Therapeutic Targeting. *Mol Cell* 79, 710-727.
- 829 2. Greninger, A.L., Dien Bard, J., Colgrove, R.C., Graf, E.H., Hanson, K.E., Hayden, M.K., Humphries, R.M.,  
830 Lowe, C.F., Miller, M.B., Pillai, D.R., *et al.* (2022). Clinical and Infection Prevention Applications of Severe

- 831 Acute Respiratory Syndrome Coronavirus 2 Genotyping: an Infectious Diseases Society of  
832 America/American Society for Microbiology Consensus Review Document. *J Clin Microbiol* 60,  
833 e0165921.
- 834 3. Obermeyer, F., Jankowiak, M., Barkas, N., Schaffner, S.F., Pyle, J.D., Yurkovetskiy, L., Bosso, M., Park,  
835 D.J., Babadi, M., MacInnis, B.L., *et al.* (2022). Analysis of 6.4 million SARS-CoV-2 genomes identifies  
836 mutations associated with fitness. *Science* 376, 1327-1332.
- 837 4. Sadeghalvad, M., Mansourabadi, A.H., Noori, M., Nejadghaderi, S.A., Masoomikarimi, M.,  
838 Alimohammadi, M., and Rezaei, N. (2022). Recent developments in SARS-CoV-2 vaccines: A systematic  
839 review of the current studies. *Rev Med Virol*, e2359.
- 840 5. Focosi, D., McConnell, S., Casadevall, A., Cappello, E., Valdiserra, G., and Tuccori, M. (2022).  
841 Monoclonal antibody therapies against SARS-CoV-2. *Lancet Infect Dis*.
- 842 6. Walls, A.C., Tortorici, M.A., Snijder, J., Xiong, X., Bosch, B.J., Rey, F.A., and Velesler, D. (2017). Tectonic  
843 conformational changes of a coronavirus spike glycoprotein promote membrane fusion. *Proc Natl Acad*  
844 *Sci U S A* 114, 11157-11162.
- 845 7. Lok, S.M. (2021). An NTD supersite of attack. *Cell Host Microbe* 29, 744-746.
- 846 8. Niu, L., Wittrock, K.N., Clabaugh, G.C., Srivastava, V., and Cho, M.W. (2021). A Structural Landscape of  
847 Neutralizing Antibodies Against SARS-CoV-2 Receptor Binding Domain. *Front Immunol* 12, 647934.
- 848 9. Piccoli, L., Park, Y.J., Tortorici, M.A., Czudnochowski, N., Walls, A.C., Beltramello, M., Silacci-Fregni, C.,  
849 Pinto, D., Rosen, L.E., Bowen, J.E., *et al.* (2020). Mapping Neutralizing and Immunodominant Sites on the  
850 SARS-CoV-2 Spike Receptor-Binding Domain by Structure-Guided High-Resolution Serology. *Cell* 183,  
851 1024-1042 e1021.
- 852 10. Corti, D., Purcell, L.A., Snell, G., and Velesler, D. (2021). Tackling COVID-19 with neutralizing  
853 monoclonal antibodies. *Cell* 184, 3086-3108.
- 854 11. Zahradnik, J., Marciano, S., Shemesh, M., Zoler, E., Harari, D., Chiaravalli, J., Meyer, B., Rudich, Y., Li,  
855 C., Marton, I., *et al.* (2021). SARS-CoV-2 variant prediction and antiviral drug design are enabled by RBD  
856 *in vitro* evolution. *Nat Microbiol* 6, 1188-1198.
- 857 12. Tuekprakhon, A., Nutalai, R., Dijokaite-Guraliuc, A., Zhou, D., Ginn, H.M., Selvaraj, M., Liu, C.,  
858 Mentzer, A.J., Supasa, P., Duyvesteyn, H.M.E., *et al.* (2022). Antibody escape of SARS-CoV-2 Omicron  
859 BA.4 and BA.5 from vaccine and BA.1 serum. *Cell* 185, 2422-2433 e2413.
- 860 13. Supasa, P., Zhou, D., Dejnirattisai, W., Liu, C., Mentzer, A.J., Ginn, H.M., Zhao, Y., Duyvesteyn, H.M.E.,  
861 Nutalai, R., Tuekprakhon, A., *et al.* (2021). Reduced neutralization of SARS-CoV-2 B.1.1.7 variant by  
862 convalescent and vaccine sera. *Cell* 184, 2201-2211 e2207.
- 863 14. Liu, C., Ginn, H.M., Dejnirattisai, W., Supasa, P., Wang, B., Tuekprakhon, A., Nutalai, R., Zhou, D.,  
864 Mentzer, A.J., Zhao, Y., *et al.* (2021). Reduced neutralization of SARS-CoV-2 B.1.617 by vaccine and  
865 convalescent serum. *Cell* 184, 4220-4236 e4213.
- 866 15. Dejnirattisai, W., Huo, J., Zhou, D., Zahradnik, J., Supasa, P., Liu, C., Duyvesteyn, H.M.E., Ginn, H.M.,  
867 Mentzer, A.J., Tuekprakhon, A., *et al.* (2022). SARS-CoV-2 Omicron-B.1.1.529 leads to widespread escape  
868 from neutralizing antibody responses. *Cell* 185, 467-484 e415.
- 869 16. Zhou, D., Dejnirattisai, W., Supasa, P., Liu, C., Mentzer, A.J., Ginn, H.M., Zhao, Y., Duyvesteyn, H.M.E.,  
870 Tuekprakhon, A., Nutalai, R., *et al.* (2021). Evidence of escape of SARS-CoV-2 variant B.1.351 from  
871 natural and vaccine-induced sera. *Cell* 184, 2348-2361 e2346.



- 872 17. Dejnirattisai, W., Zhou, D., Supasa, P., Liu, C., Mentzer, A.J., Ginn, H.M., Zhao, Y., Duyvesteyn, H.M.E.,  
873 Tuekprakhon, A., Nutalai, R., *et al.* (2021). Antibody evasion by the P.1 strain of SARS-CoV-2. *Cell* *184*,  
874 2939-2954 e2939.
- 875 18. Suzuki, R., Yamasoba, D., Kimura, I., Wang, L., Kishimoto, M., Ito, J., Morioka, Y., Nao, N., Nasser, H.,  
876 Uriu, K., *et al.* (2022). Attenuated fusogenicity and pathogenicity of SARS-CoV-2 Omicron variant. *Nature*  
877 *603*, 700-705.
- 878 19. Iketani, S., Liu, L., Guo, Y., Liu, L., Chan, J.F., Huang, Y., Wang, M., Luo, Y., Yu, J., Chu, H., *et al.* (2022).  
879 Antibody evasion properties of SARS-CoV-2 Omicron sublineages. *Nature* *604*, 553-556.
- 880 20. Nutalai, R., Zhou, D., Tuekprakhon, A., Ginn, H.M., Supasa, P., Liu, C., Huo, J., Mentzer, A.J.,  
881 Duyvesteyn, H.M.E., Dijokaite-Guraliuc, A., *et al.* (2022). Potent cross-reactive antibodies following  
882 Omicron breakthrough in vaccinees. *Cell* *185*, 2116-2131 e2118.
- 883 21. Del Rio, C., and Malani, P.N. (2022). COVID-19 in 2022-The Beginning of the End or the End of the  
884 Beginning? *JAMA* *327*, 2389-2390.
- 885 22. Di Genova, C., Sampson, A., Scott, S., Cantoni, D., Mayora-Neto, M., Bentley, E., Mattiuzzo, G.,  
886 Wright, E., Dervenli, M., Auld, B., *et al.* (2020). Production, titration, neutralisation and storage of SARS-  
887 CoV-2 lentiviral pseudotypes. *figshare*.
- 888 23. Flaxman, A., Marchevsky, N.G., Jenkin, D., Aboagye, J., Aley, P.K., Angus, B., Belij-Rammerstorfer, S.,  
889 Bibi, S., Bittaye, M., Cappuccini, F., *et al.* (2021). Reactogenicity and immunogenicity after a late second  
890 dose or a third dose of ChAdOx1 nCoV-19 in the UK: a substudy of two randomised controlled trials  
891 (COV001 and COV002). *Lancet* *398*, 981-990.
- 892 24. Cele, S., Jackson, L., Khoury, D.S., Khan, K., Moyo-Gwete, T., Tegally, H., San, J.E., Cromer, D.,  
893 Scheepers, C., Amoako, D.G., *et al.* (2021). Omicron extensively but incompletely escapes Pfizer  
894 BNT162b2 neutralization. *Nature*, *602*, 654-656.
- 895 25. Weinreich, D.M., Sivapalasingam, S., Norton, T., Ali, S., Gao, H., Bhore, R., Musser, B.J., Soo, Y., Rofail,  
896 D., Im, J., *et al.* (2021). REGN-COV2, a Neutralizing Antibody Cocktail, in Outpatients with Covid-19. *N*  
897 *Engl J Med* *384*, 238-251.
- 898 26. Dong, J., Zost, S.J., Greaney, A.J., Starr, T.N., Dingens, A.S., Chen, E.C., Chen, R.E., Case, J.B., Sutton,  
899 R.E., Gilchuk, P., *et al.* (2021). Genetic and structural basis for SARS-CoV-2 variant neutralization by a  
900 two-antibody cocktail. *Nat Microbiol* *6*, 1233-1244.
- 901 27. Sun, Y., and Ho, M. (2020). Emerging antibody-based therapeutics against SARS-CoV-2 during the  
902 global pandemic. *Antib Ther* *3*, 246-256.
- 903 28. Westendorf, K., Zentelis, S., Wang, L., Foster, D., Vaillancourt, P., Wiggin, M., Lovett, E., van der Lee,  
904 R., Hendle, J., Pustilnik, A., *et al.* (2022). LY-CoV1404 (bebtelovimab) potently neutralizes SARS-CoV-2  
905 variants. *Cell Rep* *39*, 110812.
- 906 29. Xie, X., Liu, Y., Liu, J., Zhang, X., Zou, J., Fontes-Garfias, C.R., Xia, H., Swanson, K.A., Cutler, M.,  
907 Cooper, D., *et al.* (2021). Neutralization of SARS-CoV-2 spike 69/70 deletion, E484K and N501Y variants  
908 by BNT162b2 vaccine-elicited sera. *Nat Med* *27*, 620-621.
- 909 30. Liu, Y., Liu, J., Plante, K.S., Plante, J.A., Xie, X., Zhang, X., Ku, Z., An, Z., Scharton, D., Schindewolf, C.,  
910 *et al.* (2022). The N501Y spike substitution enhances SARS-CoV-2 infection and transmission. *Nature*  
911 *602*, 294-299.

- 912 31. Cui, Z., Liu, P., Wang, N., Wang, L., Fan, K., Zhu, Q., Wang, K., Chen, R., Feng, R., Jia, Z., *et al.* (2022).  
913 Structural and functional characterizations of infectivity and immune evasion of SARS-CoV-2 Omicron.  
914 *Cell* *185*, 860-871 e813.
- 915 32. Hui, K.P.Y., Ho, J.C.W., Cheung, M.C., Ng, K.C., Ching, R.H.H., Lai, K.L., Kam, T.T., Gu, H., Sit, K.Y., Hsin,  
916 M.K.Y., *et al.* (2022). SARS-CoV-2 Omicron variant replication in human bronchus and lung *ex vivo*.  
917 *Nature* *603*, 715-720.
- 918 33. Meng, B., Abdullahi, A., Ferreira, I., Goonawardane, N., Saito, A., Kimura, I., Yamasoba, D., Gerber,  
919 P.P., Fatihi, S., Rathore, S., *et al.* (2022). Altered TMPRSS2 usage by SARS-CoV-2 Omicron impacts  
920 infectivity and fusogenicity. *Nature* *603*, 706-714.
- 921 34. Folegatti, P.M., Ewer, K.J., Aley, P.K., Angus, B., Becker, S., Belij-Rammerstorfer, S., Bellamy, D., Bibi,  
922 S., Bittaye, M., Clutterbuck, E.A., *et al.* (2020). Safety and immunogenicity of the ChAdOx1 nCoV-19  
923 vaccine against SARS-CoV-2: a preliminary report of a phase 1/2, single-blind, randomised controlled  
924 trial. *Lancet* *396*, 467-478.
- 925 35. Nie, L., Qin, H., Wang, M., Lu, Q., Li, X., Sun, Q., Liu, J., Fan, C., Huang, W., Xu, M., *et al.* (2020)  
926 Establishment and validation of a pseudovirus neutralization assay for SARS-CoV-2. *Emerg Microbes*  
927 *Infect.* *9*, 680-686.
- 928 36. Huo, J., Le Bas, A., Ruza, R.R., Duyvesteyn, H.M.E., Mikolajek, H., Malinauskas, T., Tan, T.K., Rijal, P.,  
929 Dumoux, M., Ward, P.N., *et al.* (2020). Neutralizing nanobodies bind SARS-CoV-2 spike RBD and block  
930 interaction with ACE2. *Nature structural & molecular biology* *27*, 846-854.
- 931 37. Walter, T.S., Diprose, J., Brown, J., Pickford, M., Owens, R.J., Stuart, D.I., and Harlos, K. (2003). A  
932 procedure for setting up high-throughput nanolitre crystallization experiments. I. Protocol design and  
933 validation. *Journal of Applied Crystallography* *36*, 308-314.
- 934 38. Winter, G. (2010). xia2: an expert system for macromolecular crystallography data reduction. *Journal*  
935 *of applied crystallography* *43*, 186-190.
- 936 39. Winter, G., Waterman, D.G., Parkhurst, J.M., Brewster, A.S., Gildea, R.J., Gerstel, M., Fuentes-  
937 Montero, L., Vollmar, M., Michels-Clark, T., Young, I.D., *et al.* (2018). DIALS: implementation and  
938 evaluation of a new integration package. *Acta Crystallogr D Struct Biol* *74*, 85-97.
- 939 40. Emsley, P., Lohkamp, B., Scott, W.G., and Cowtan, K. (2010). Features and development of Coot. *Acta*  
940 *Crystallographica Section D: Biological Crystallography* *66*, 486-501.
- 941 41. Liebschner, D., Afonine, P.V., Baker, M.L., Bunkoczi, G., Chen, V.B., Croll, T.I., Hintze, B., Hung, L.W.,  
942 Jain, S., McCoy, A.J., *et al.* (2019). Macromolecular structure determination using X-rays, neutrons and  
943 electrons: recent developments in Phenix. *Acta Crystallogr D Struct Biol* *75*, 861-877.
- 944 42. Stuart, D.I., Levine, M., Muirhead, H., and Stammers, D.K. (1979). Crystal structure of cat muscle  
945 pyruvate kinase at a resolution of 2.6 Å. *J Mol Biol* *134*, 109-142.
- 946 43. Aricescu, A.R., Lu, W., and Jones, E.Y. (2006). A time- and cost-efficient system for high-level protein  
947 production in mammalian cells. *Acta Crystallogr D Biol Crystallogr* *62*, 1243-1250.
- 948 44. Stewart, S.A., Dykxhoorn, D.M., Palliser, D., Mizuno, H., Yu, E.Y., An, D.S., Sabatini, D.M., Chen, I.S.,  
949 Hahn, W.C., Sharp, P.A., *et al.* (2003). Lentivirus-delivered stable gene silencing by RNAi in primary cells.  
950 *RNA* *9*, 493-501.
- 951 45. Nettleship, J.E., Ren, J., Rahman, N., Berrow, N.S., Hatherley, D., Barclay, A.N., and Owens, R.J.  
952 (2008). A pipeline for the production of antibody fragments for structural studies using transient  
953 expression in HEK 293T cells. *Protein Expr Purif* *62*, 83-89.

954 46. Delano, W.L. (2004) The PyMOL molecular graphics system. DeLano Scientific, San Carlos,  
955 USA.<http://pymol.sourceforge.net/>

Journal Pre-proof

A

BA.1	A67V,Δ69-70,T95I,G142D,Δ143-145,	N211I,Δ212,	ins214EPE
BA.1.1	A67V,Δ69-70,T95I,G142D,Δ143-145,	N211I,Δ212,	ins214EPE
BA.2	T19I,Δ24-26,A27S,	G142D,	V213G
BA.2.75	T19I,Δ24-26,A27S,	G142D,	W152R,F157L,I210V, V213G, G257S
BA.3	A67V,Δ69-70,T95I,G142D, Δ143-145,	N211I,Δ212	
BA.4/5	T19I,Δ24-26,A27S, Δ69-70, G142D,	V213G	
BA.1	G339D, S371L,S373P,S375F,	K417N,N440K,G446S	
BA.1.1	G339D,R346K,S371L,S373P,S375F,	K417N,N440K,G446S	
BA.2	G339D, S371F,S373P,S375F,T376A,D405N,R408S,	K417N,N440K	
BA.2.75	G339H, S371F,S373P,S375F,T376A,D405N,R408S,	K417N,N440K,G446S	
BA.3	G339D, S371F,S373P,S375F, D405N,	K417N,N440K,G446S	
BA.4/5	G339D, S371F,S373P,S375F,T376A,D405N,R408S,	K417N,N440K	
BA.1	S477N,T478K, E484A,	Q493R,G496S,Q498R,N501Y,Y505H	
BA.1.1	S477N,T478K,E484A,	Q493R,G496S,Q498R,N501Y,Y505H	
BA.2	S477N,T478K,E484A,	Q493R, Q498R,N501Y,Y505H	
BA.2.75	N460K,S477N,T478K,E484A,	Q498R,N501Y,Y505H	
BA.3	S477N,T478K,E484A,	Q493R, Q498R,N501Y,Y505H	
BA.4/5	L452R, S477N,T478K E484A,F486V,	Q498R,N501Y,Y505H	
BA.1	T547K,D614G,H655Y,N679K,P681H,N764K,D796Y,N856K,Q954H,N969K,L981F		
BA.1.1	T547K,D614G,H655Y,N679K,P681H,N764K,D796Y,N856K,Q954H,N969K,L981F		
BA.2	D614G,H655Y,N679K,P681H,N764K,D796Y,	Q954H,N969K	
BA.2.75	D614G,H655Y,N679K,P681H,N764K,D796Y,	Q954H,N969K	
BA.3	D614G,H655Y,N679K,P681H,N764K,D796Y,	Q954H,N969K	
BA.4/5	D614G,H655Y,N679K,P681H,N764K,D796Y,	Q954H,N969K	

B

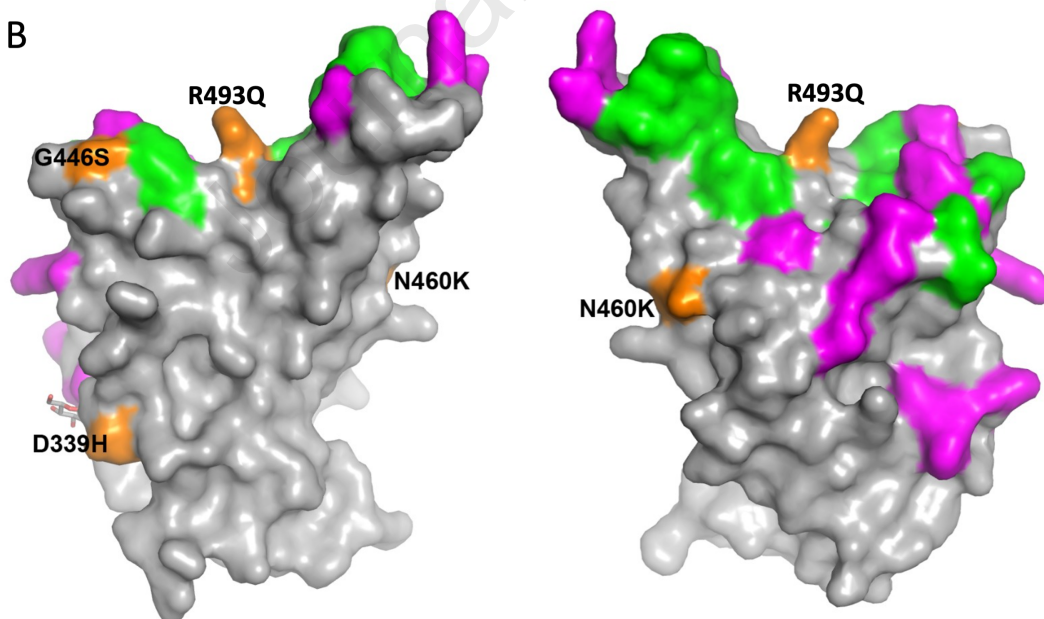


Figure 1

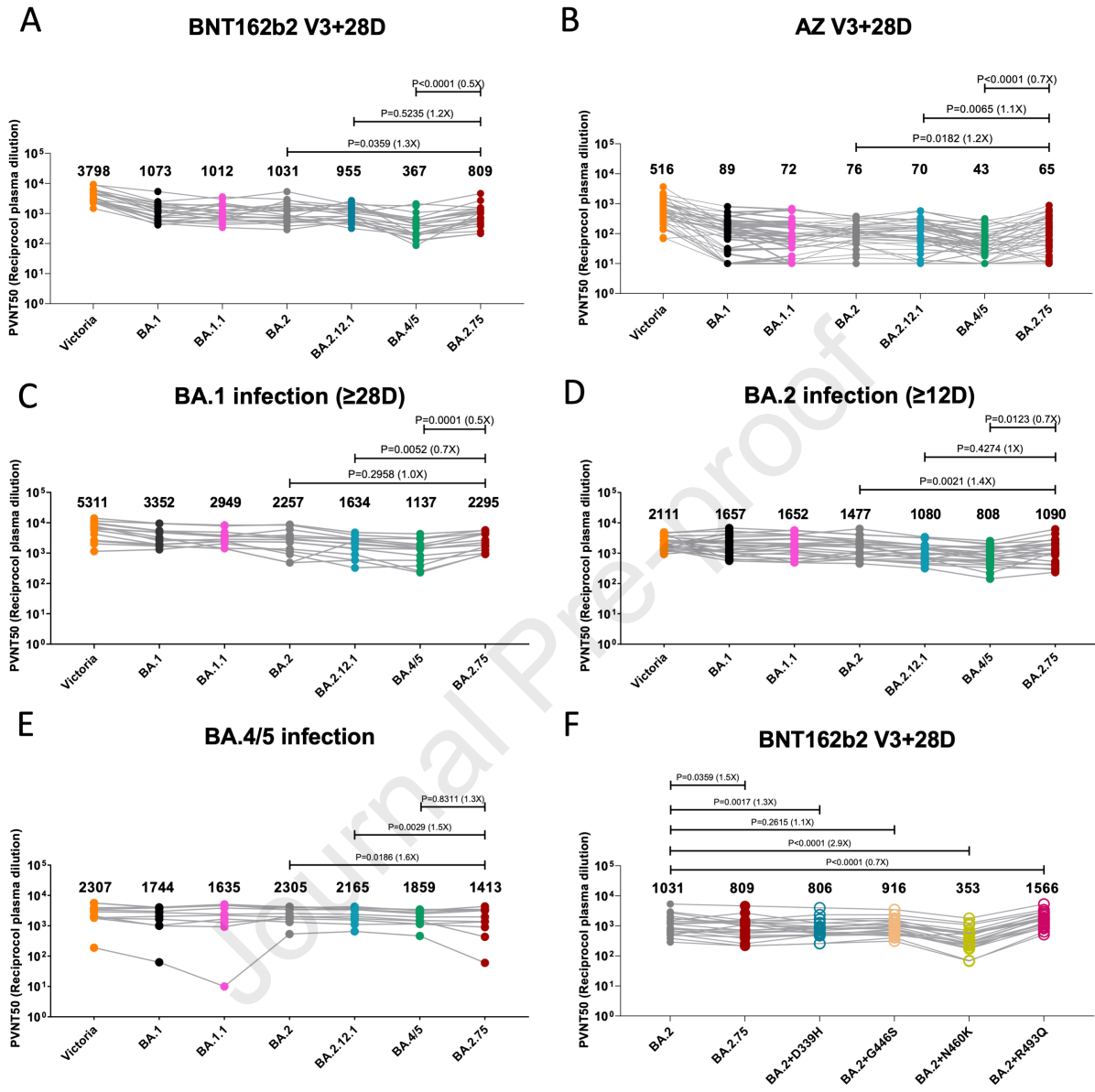


Figure 2

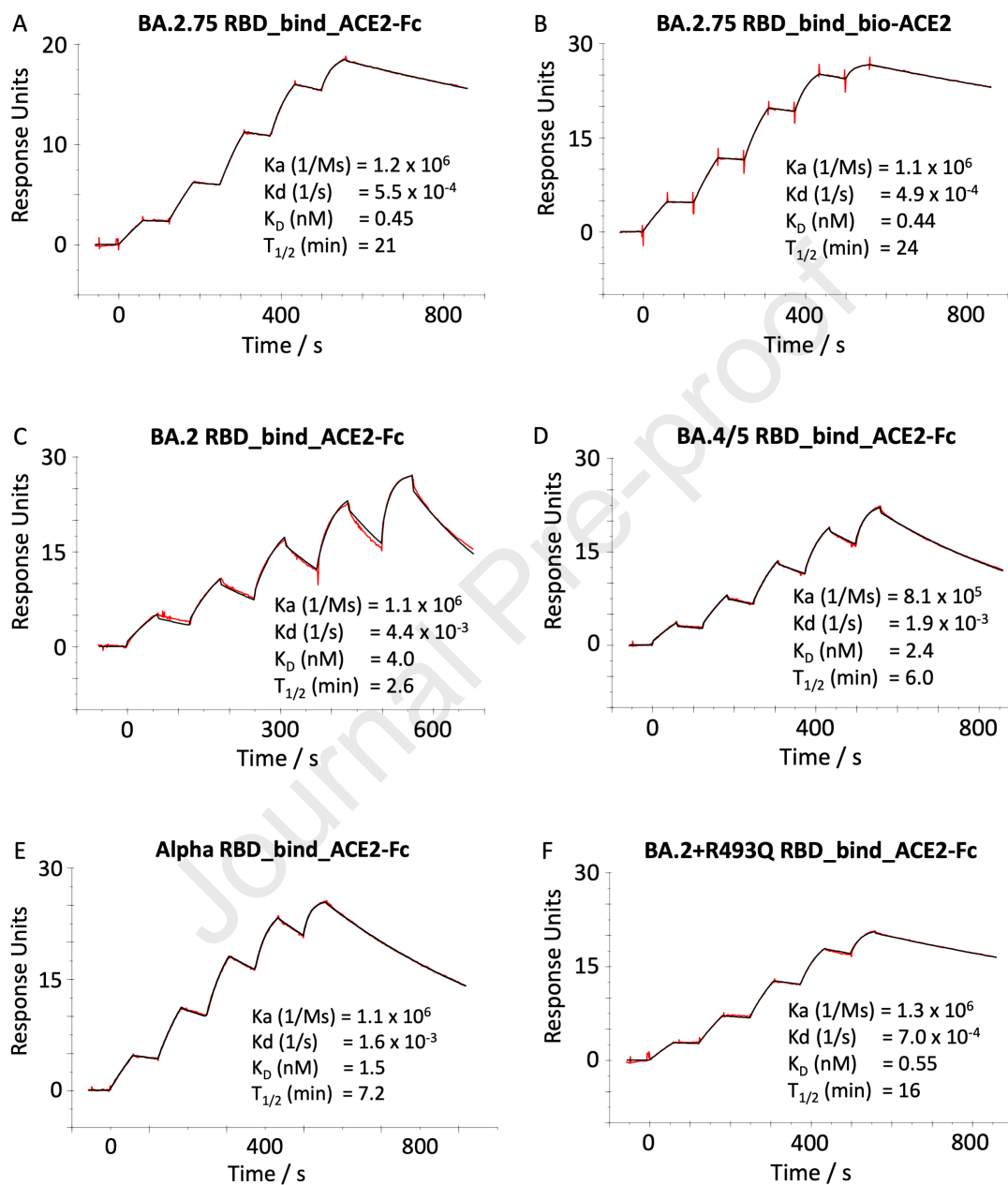


Figure 3

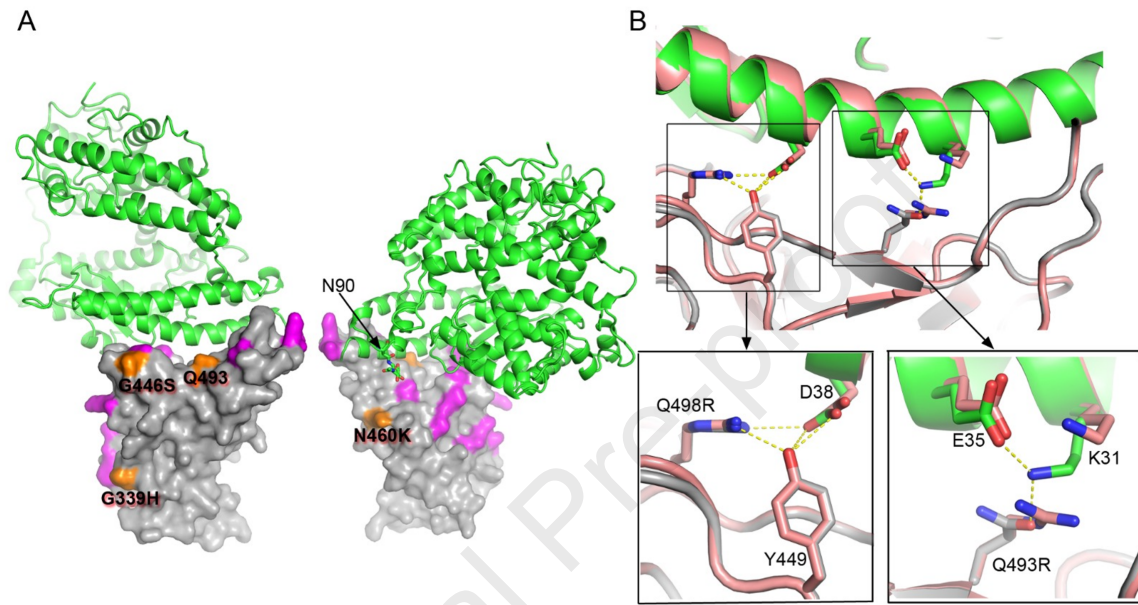
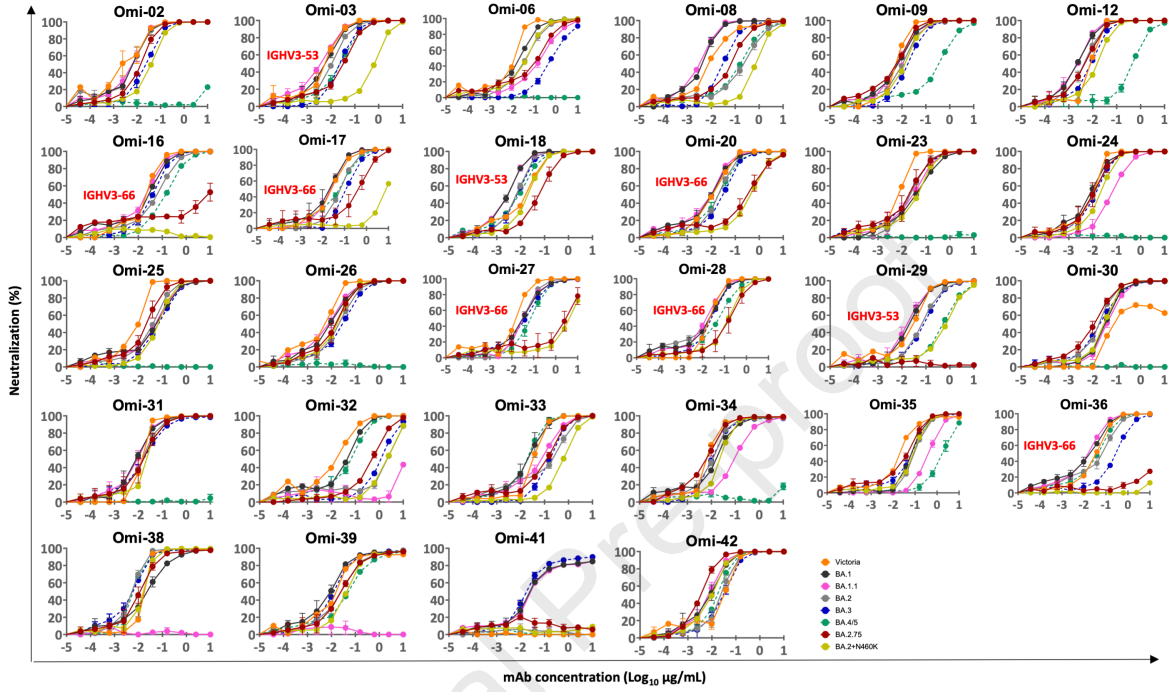


Figure 4



A



B

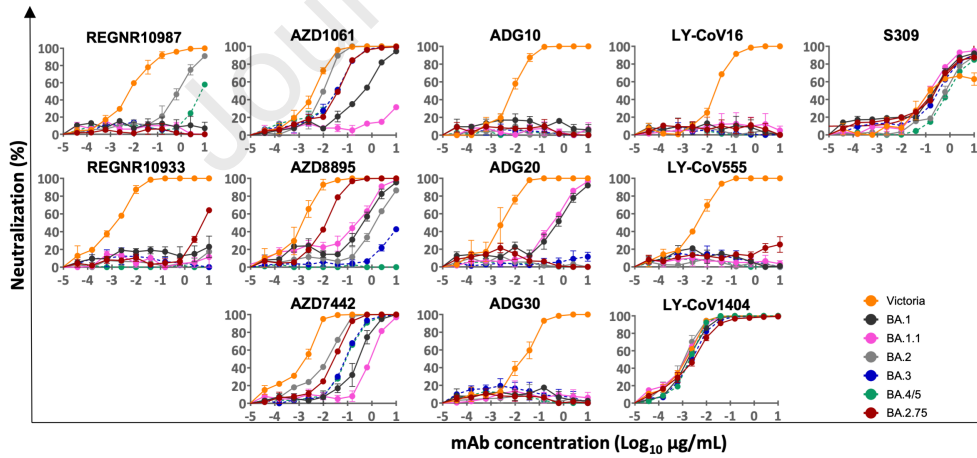


Figure 5



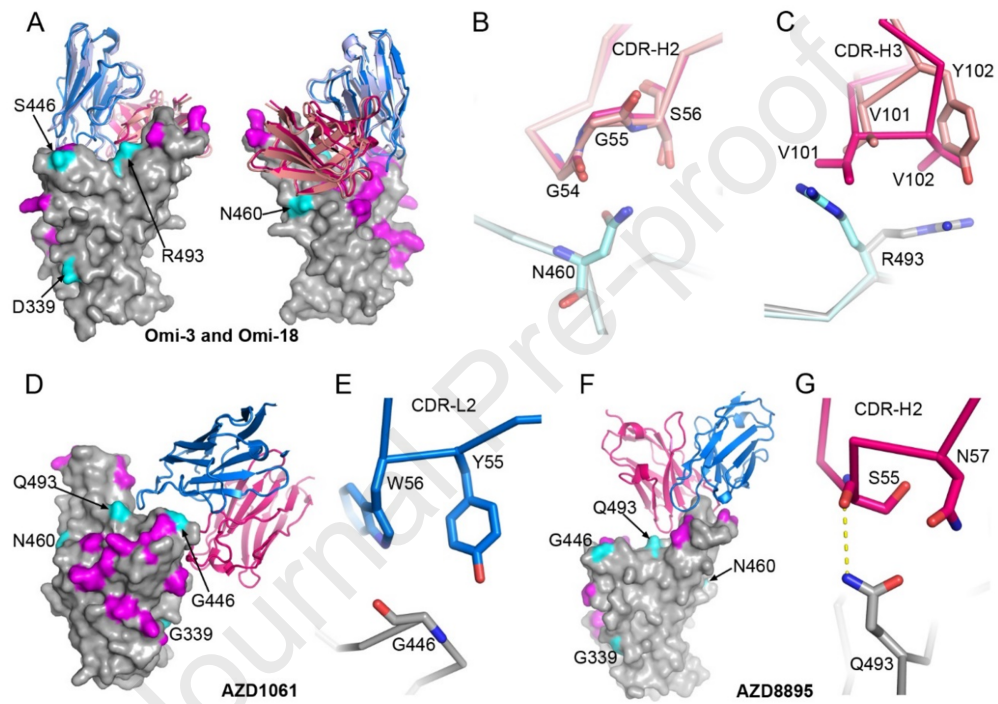


Figure 6

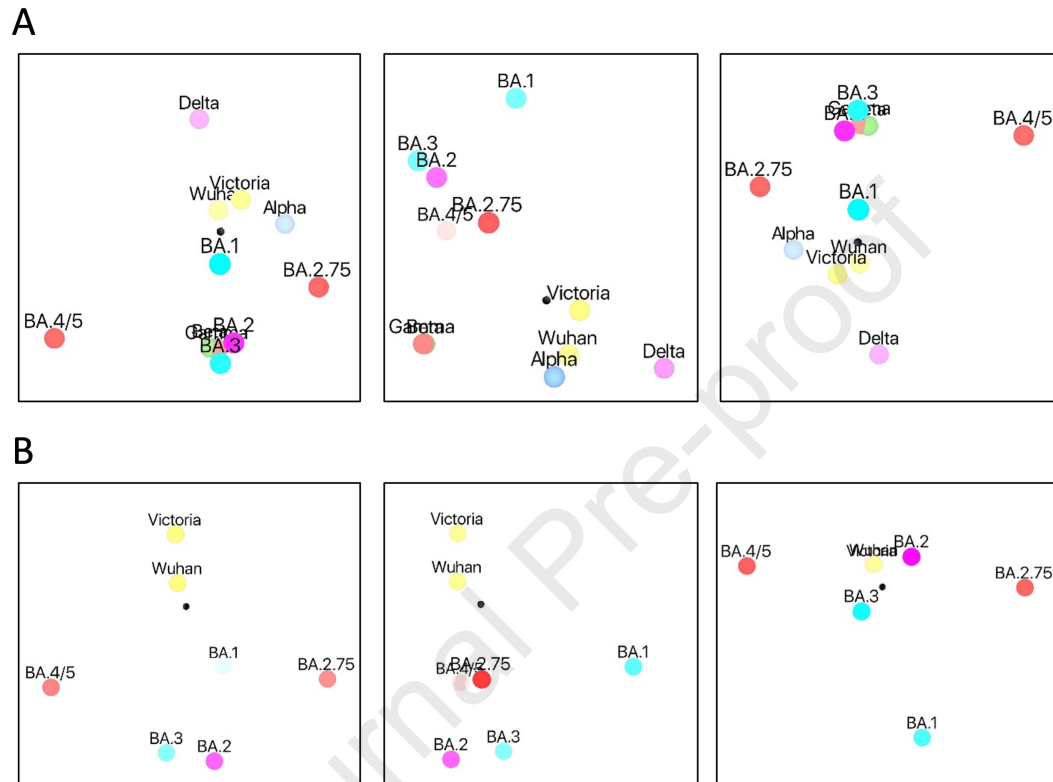


Figure 7

## Highlights

- BA.2.75 affinity for ACE2 is increased 9-fold compared to BA.2.
- N460K increases neutralization escape and likely increases ACE2 affinity.
- The revertant R493Q decreases neutralization escape but increases ACE2 affinity.
- Affinity to ACE2 appears to be prioritized over neutralization escape.

## eTOC Blurb

Huo et al. characterize the SARS-CoV-2 variant BA.2.75 (originally identified in India). Its affinity for ACE2 is increased 9-fold over BA.2 and there is evidence of escape of BA.2.75 from immune serum, particularly from Delta infection. ACE2 affinity appears to be prioritized over greater escape via the R493Q reversion mutation.

## KEY RESOURCES TABLE

REAGENT or RESOURCE	SOURCE	IDENTIFIER
<b>Antibodies</b>		
Fab	Dejnirattisai et al. 2021 (ref 17)	N/A
IgG	Dejnirattisai et al. 2021 and Liu et al 2021 (refs 17,14)	N/A
Human anti-NP (mAb 206)	Dejnirattisai et al. 2021 (ref 17)	N/A
Regeneron mAbs	AstraZeneca	Cat#REGN10933 and REGN10987
AstraZeneca mAbs	AstraZeneca	Cat#AZD1061, AZD8895 and AZD7442
Vir mAbs	Adagio	Cat#S309
Lilly mAbs	Adagio	Cat#Ly-CoV555, Ly-CoV16 and Ly-CoV1404
Adagio mAbs	Adagio	Cat#ADG10, ADG20 and ADG30
Omicron antibodies	Nutalai et al., 2022 (ref 20)	N/A
<b>Bacterial, Virus Strains, and Yeast</b>		
DH5 $\alpha$ bacteria	In Vitrogen	Cat#18263012
<b>Biological Samples</b>		
Serum from Pfizer-vaccinated individuals	University of Oxford	N/A
Serum from AstraZeneca-Oxford-vaccinated individuals	University of Oxford	N/A
Plasma from SARS-CoV-2 patients	John Radcliffe Hospital in Oxford UK, South Africa, and FIOCRUZ (WHO) Brazil	N/A
<b>Chemicals, Peptides, and Recombinant Proteins</b>		
His-tagged SARS-CoV-2 RBD	Dejnirattisai et al. 2021 (ref 17)	N/A
His-tagged Avi-tagged SARS-CoV-2/BA.2.75 RBD	This paper	N/A
His-tagged SARS-CoV-2/BA.2+R493Q RBD	This paper	N/A
His-tagged SARS-CoV-2/BA.2 RBD	Nutalai et al., 2022 (ref 20)	N/A
His-tagged SARS-CoV-2/BA.4/5 RBD	Tuekprakhon et al., 2022 (ref 12)	N/A
His-tagged SARS-CoV-2/Alpha RBD	Supasa et al., 2021 (ref 13)	N/A
Human ACE2-hlgG1Fc	Liu et al. 2021 (ref 14)	N/A
Phosphate buffered saline tablets	Sigma-Aldrich	Cat#P4417
Dulbecco's Modified Eagle Medium, high glucose	Sigma-Aldrich	Cat#D5796
Dulbecco's Modified Eagle Medium, low glucose	Sigma-Aldrich	Cat#D6046
FreeStyle™ 293 Expression Medium	Gibco	Cat#12338018
L-Glutamine–Penicillin–Streptomycin solution	Sigma-Aldrich	Cat#G1146
GlutaMAX™ Supplement	Gibco	Cat#35050061
UltraDOMA PF Protein-free Medium	Lonza	Cat#12-727F

Opti-MEM™	Gibco	Cat#11058021
Fetal Bovine Serum	Gibco	Cat#12676029
Strep-Tactin®XT	IBA Lifesciences	Cat#2-1206-025
HEPES	Melford	Cat#34587-39108
LB broth	Fisher Scientific UK	Cat#51577-51656
Trypsin-EDTA	Gibco	Cat#2259288
TrypLE™ Express Enzyme	Gibco	Cat#12604013
L-Glutamine 200 mM (100X)	Gibco	Cat#2036885
Isopropyl β-d-1-thiogalactopyranoside	Meridian Bioscience	Cat#BIO-37036
Kanamycin	Melford	Cat#K22000
Ampicillin	Sigma-Aldrich	Cat#PHR2838
Agarose	Sigma-Aldrich	Cat#A2929
SYBR™ Safe DNA Gel Stain	Fisher Scientific UK	Cat#S33102
QIAprep Spin Miniprep Kit	Qiagen	Cat#27106X4
QIAquick® PCR & Gel Cleanup Kit	Qiagen	Cat#28704
Phusion™ High-Fidelity DNA Polymerase	Fisher Scientific UK	Cat#F530S
Bright-Glo™ Luciferase Assay System	Promega	Cat#E2620
HIV1 p24 ELISA Kit	Abcam	Cat#ab218268
NaCl	Sigma-Aldrich	Cat#S9888
Sensor Chip Protein A	Cytiva	Cat#29127555
Biotin CAPture Kit, Series S	Cytiva	CAT#28920234
HBS-EP+ Buffer 10×	Cytiva	Cat# BR100669
Regeneration Solution (glycine-HCl pH 1.7)	Cytiva	Cat# BR100838
<b>Deposited Data</b>		
Crystal structures of SARS-CoV-2 Omicron BA.2.75 RBD in complex with ACE2	This paper	PDB: 8ASY
<b>Experimental Models: Cell Lines</b>		
HEK293 cells	ATCC	Cat#CRL-3216
Expi293F™ Cells	Gibco,	Cat#A14527
HEK293T/17 cells	ATCC	Cat#CRL-11268™
HEK293T cells	ATCC	Cat#CRL-11268
Vero CCL-81 cells	ATCC	Cat#CCL-81
VeroE6/TMPRSS2 cells	NIBSC	Ref. no. 100978
<b>Recombinant DNA</b>		
Vector: pHLsec	Aricescu et al., 2006 (ref 43)	N/A
Vector: pNEO	Aricescu et al., 2006 (ref 43)	N/A
Vector: pHLsec-SARS-CoV-2 spike of Omicron	Nutalai et al., 2022 (ref 20)	N/A
Vector: pOPINTTGneo-BAP-SARS-CoV-2 RBD of BA.2.75	This paper	N/A
Vector: pNEO-SARS-CoV-2 RBD of BA.2	Nutalai et al., 2022 (ref 20)	N/A
Vector: pNEO-SARS-CoV-2 RBD of BA.4/5	Tuekprakhon et al., 2022 (ref 12)	N/A
Vector: pNEO-SARS-CoV-2 RBD of BA.2+R493Q	This paper	N/A
Vector: pNEO-SARS-CoV-2 RBD of Alpha	Supasa et al., 2021 (ref 13)	N/A

Vector: pCMV-VSV-G	Stewart et al. 2003 (ref 44)	Addgene plasmid # 8454
pHR-SIN-ACE2	Alain Townsend, Oxford	N/A
Vector: pOPING-ET	Nettleship et al., 2008 (ref 45)	N/A
Vector: pcDNA-SARS-CoV-2 spike of Victoria strain (S247R)	Liu et al., 2021 (ref 14)	N/A
Vector: pcDNA-SARS-CoV-2 spike of BA.1 strain (A67V, Δ69-70, T95I, G142D/Δ143-145, Δ211/L212I, ins214EPE, G339D, S371L, S373P, S375F, K417N, N440K, G446S, S477N, T478K, E484A, Q493R, G496S, Q498R, N501Y, Y505H, T547K, D614G, H655Y, N679K, P681H, N764K, D796Y, N856K, Q954H, N969K, L981F)	Nutalai et al., 2022 (ref 20)	N/A
Vector: pcDNA-SARS-CoV-2 spike of BA.1.1 strain (A67V, Δ69-70, T95I, G142D/Δ143-145, Δ211/L212I, ins214EPE, G339D, R346K, S371L, S373P, S375F, K417N, N440K, G446S, S477N, T478K, E484A, Q493R, G496S, Q498R, N501Y, Y505H, T547K, D614G, H655Y, N679K, P681H, N764K, D796Y, N856K, Q954H, N969K, L981F)	Nutalai et al., 2022 (ref 20)	N/A
Vector: pcDNA-SARS-CoV-2 spike of BA.2 strain (T19I, Δ24-26, A27S, G142D, V213G, G339D, S371F, S373P, S375F, T376A, D405N, R408S, K417N, N440K, S477N, T478K, E484A, Q493R, Q498R, N501Y, Y505H, D614G, H655Y, N679K, P681H, N764K, D796Y, Q954H, N969K)	Nutalai et al., 2022 (ref 20)	N/A
Vector: pcDNA-SARS-CoV-2 spike of BA.2.12.1 strain (T19I, Δ24-26, A27S, G142D, V213G, G339D, S371F, S373P, S375F, T376A, D405N, R408S, K417N, N440K, L452Q, S477N, T478K, E484A, Q493R, Q498R, N501Y, Y505H, D614G, H655Y, N679K, P681H, S704L, N764K, D796Y, Q954H, N969K)	Nutalai et al., 2022 (ref 20)	N/A
Vector: pcDNA-SARS-CoV-2 spike of BA.4/5 strain (T19I, Δ24-26, A27S, Δ69-70, G142D, V213G, G339D, S371F, S373P, S375F, T376A, D405N, R408S, K417N, N440K, L452R, S477N, T478K, E484A, F486V, Q498R, N501Y, Y505H, D614G, H655Y, N679K, P681H, N764K, D796Y, Q954H, N969K)	Tuekprakhon et al., 2022 (ref 12)	N/A
Vector: pcDNA-SARS-CoV-2 spike of BA.2.75 strain (T19I, Δ24-26, A27S, G142D, K147E, W152R, F157L, I210V, V213G, G257S, D339H, S371F, S373P, S375F, T376A, D405N, R408S, K417N, N440K, G446S, N460K, S477N, T478K, E484A, R493Q, Q498R, N501Y, Y505H, D614G, H655Y, N679K, P681H, N764K, D796Y, Q954H, N969K)	This paper	N/A
Vector: pcDNA-SARS-CoV-2 spike of BA.2+D339H strain (T19I, Δ24-26, A27S, G142D, V213G, D339H, S371F, S373P, S375F, T376A, D405N, R408S, K417N, N440K, S477N, T478K, E484A,	This paper	N/A

Q493R, Q498R, N501Y, Y505H, D614G, H655Y, N679K, P681H, N764K, D796Y, Q954H, N969K)		
Vector: pcDNA-SARS-CoV-2 spike of BA.2+R493Q strain (T19I, Δ24-26, A27S, G142D, V213G, G339D, S371F, S373P, S375F, T376A, D405N, R408S, K417N, N440K, S477N, T478K, E484A, R493Q, Q498R, N501Y, Y505H, D614G, H655Y, N679K, P681H, N764K, D796Y, Q954H, N969K)	This paper	N/A
Vector: pcDNA-SARS-CoV-2 spike of BA.2+G446S strain (T19I, Δ24-26, A27S, G142D, V213G, G339D, S371F, S373P, S375F, T376A, D405N, R408S, K417N, N440K, G446S, S477N, T478K, E484A, Q493R, Q498R, N501Y, Y505H, D614G, H655Y, N679K, P681H, N764K, D796Y, Q954H, N969K)	This paper	N/A
Vector: human IgG1 heavy chain	German Cancer Research Center, Heidelberg, Germany (H. Wardemann)	N/A
Vector: human lambda light chain	German Cancer Research Center, Heidelberg, Germany (H. Wardemann)	N/A
Vector: human kappa light chain	German Cancer Research Center, Heidelberg, Germany (H. Wardemann)	N/A
Vector: Human Fab	Univeristy of Oxford	N/A
Vector: pJYDC1	Adgene	ID: 162458
TM149 BirA pDisplay	University of Oxford, NDM (C. Siebold)	N/A
<b>Software and Algorithms</b>		
COOT	Emsley et al., 2010 (ref 40)	<a href="https://www2.mrc-lmb.cam.ac.uk/personal/pemsley/coot/">https://www2.mrc-lmb.cam.ac.uk/personal/pemsley/coot/</a>
Xia2-dials	Winter et al., 2018 (ref 39)	<a href="https://xia2.github.io/parameters.html">https://xia2.github.io/parameters.html</a>
PHENIX	Liebschner et al., 2019 (ref 41)	<a href="https://www.phenix-online.org/">https://www.phenix-online.org/</a>
PyMOL	Warren DeLano, 2004 (ref 46)	<a href="https://pymol.org/">https://pymol.org/</a>
Data Acquisition Software 11.1.0.11	Fortebio	<a href="https://www.fortebio.com/products/octet-systems-software">https://www.fortebio.com/products/octet-systems-software</a>
Data Analysis Software HT 11.1.0.25	Fortebio	<a href="https://www.fortebio.com/products/octet-systems-software">https://www.fortebio.com/products/octet-systems-software</a>
Prism 9.0	GraphPad	<a href="https://www.graphpad.com/scientific-software/prism/">https://www.graphpad.com/scientific-software/prism/</a>
Yeast display titration curve fitting were done by the standard non-cooperative Hill equation, fitted by	Zahradnik et al., 2021 (ref 11)	N/A

nonlinear least-squares regression with two additional parameters using Python 3.7		
IBM SPSS Software 27	IBM	<a href="https://www.ibm.com">https://www.ibm.com</a>
Mabscape	This paper	<a href="https://github.com/helenginn/mabscape">https://github.com/helenginn/mabscape</a> <a href="https://snapcraft.io/mabscape">https://snapcraft.io/mabscape</a>
Biacore T200 Evaluation Software 3.1	Cytiva	<a href="http://www.cytivalifesciences.com">www.cytivalifesciences.com</a>
<b>Other</b>		
X-ray data were collected at beamline I03, Diamond Light Source, under proposal ib27009 for COVID-19 rapid access	This paper	<a href="https://www.diamond.ac.uk/covid-19/for-scientists/rapid-access.html">https://www.diamond.ac.uk/covid-19/for-scientists/rapid-access.html</a>
TALON® Superflow Metal Affinity Resin	Clontech	Cat#635668
HiLoad® 16/600 Superdex® 200 pg	Cytiva	Cat#28-9893-35
Superdex 200 increase 10/300 GL column	Cytiva	Cat#28990944
HisTrap nickel HP 5-ml column	Cytiva	Cat#17524802
HiTrap Heparin HT 5-ml column	Cytiva	Cat#17040703
Amine Reactive Second-Generation (AR2G) Biosensors	Fortebio	Cat#18-5092
Octet RED96e	Fortebio	<a href="https://www.fortebio.com/products/label-free-bi-detection/8-channel-octet-systems">https://www.fortebio.com/products/label-free-bi-detection/8-channel-octet-systems</a>
Buffer exchange system “QuixStand”	GE Healthcare	Cat#56-4107-78
Cartesian dispensing system	Genomic solutions	Cat#MIC4000
Hydra-96	Robbins Scientific	Cat#Hydra-96
96-well crystallization plate	Greiner bio-one	Cat#E20113NN
Crystallization Imaging System	Formulatrix	Cat#RI-1000
Sonics vibra-cell vcx500 sonicator	VWR	Cat#432-0137
Biacore T200	Cytiva	<a href="https://www.cytivalifesciences.com/en/us/shop/prot ein-analysis/spr-label-free-analysis/systems/biacore-t200-p-05644">https://www.cytivalifesciences.com/en/us/shop/prot ein-analysis/spr-label-free-analysis/systems/biacore-t200-p-05644</a>



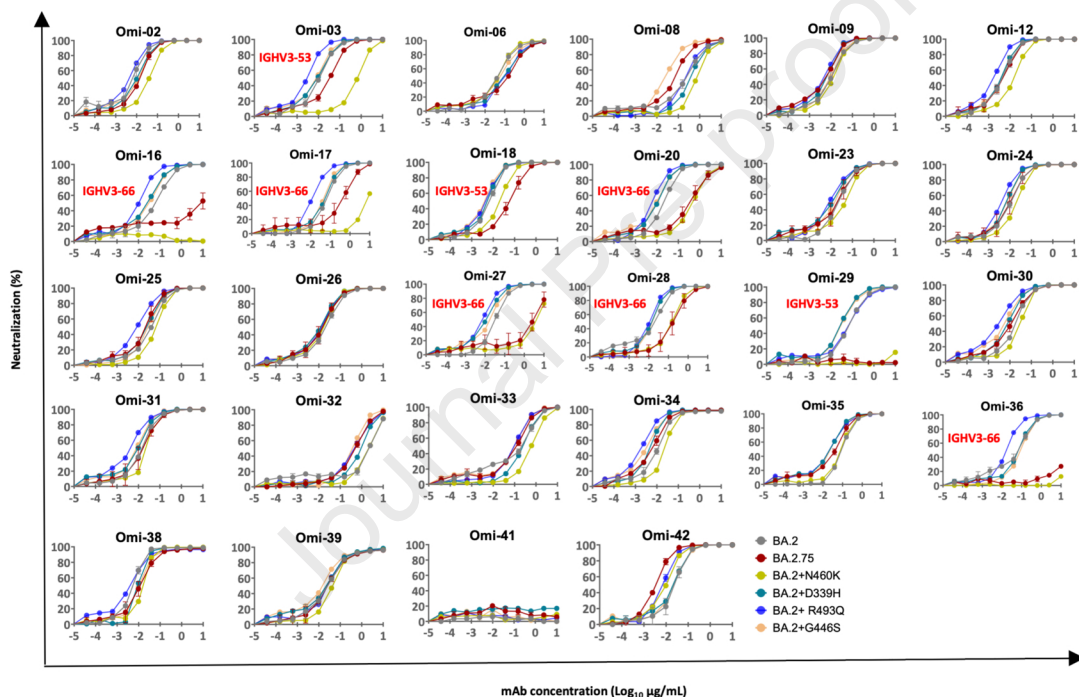


**Figure S1 Pseudoviral neutralization assays against monoclonal antibodies.** (A) Neutralization curves for a panel of 28 monoclonal antibodies made from samples taken from vaccinees infected with BA.1. Titration curves for single mutations of BA.2.27 in the BA.2 background are compared with BA.2 and BA.2.75. IC50 titres are shown in Table S2. Related to Figure 5. All assays have been done at least twice.

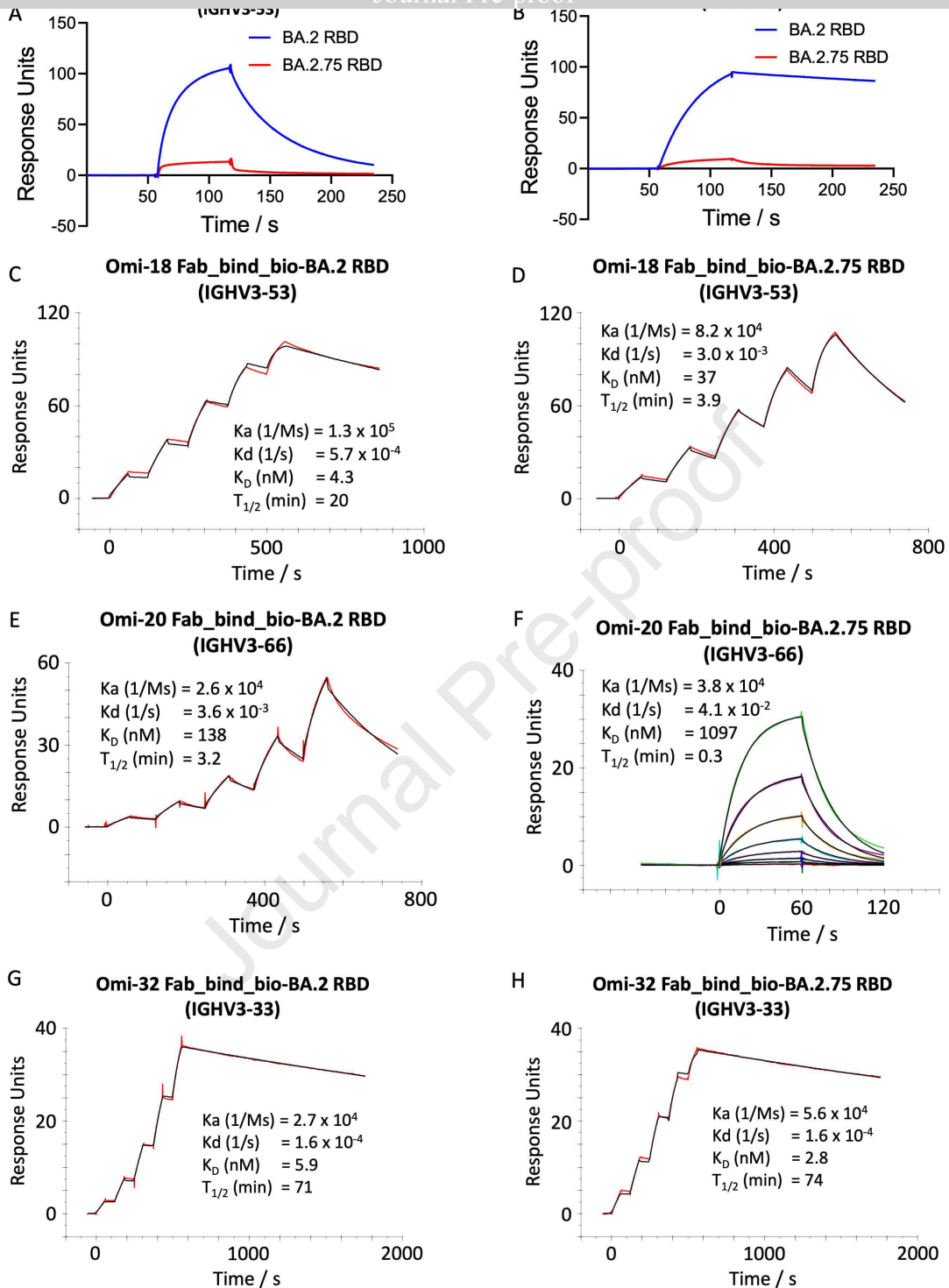


**Figure S2 Surface plasmon resonance (SPR) analysis of interaction between BA.2 or BA.2.75 RBD and selected mAbs.** (A) Binding of Omi-29 (IGHV3-53) to BA.2.75 RBD is severely reduced compared to that of BA.2, as shown by a single-injection of 1  $\mu$ M Omi-29 Fab over sample flow cells containing biotinylated BA.2 or BA.2.75 RBD. (B) Binding of Omi-36 (IGHV3-66) to BA.2.75 RBD is severely reduced compared to that of BA.2, as shown by a single-injection of 0.2  $\mu$ M BA.2 or BA.2.75 RBD over sample flow cells containing Omi-36 in the IgG form. (C-H) Sensorgrams (Red / Coloured: original binding curve; black: fitted curve) showing the interactions between BA.2 or BA.4/5 RBD and selected mAbs, with kinetics data shown. Related to Figure 5.

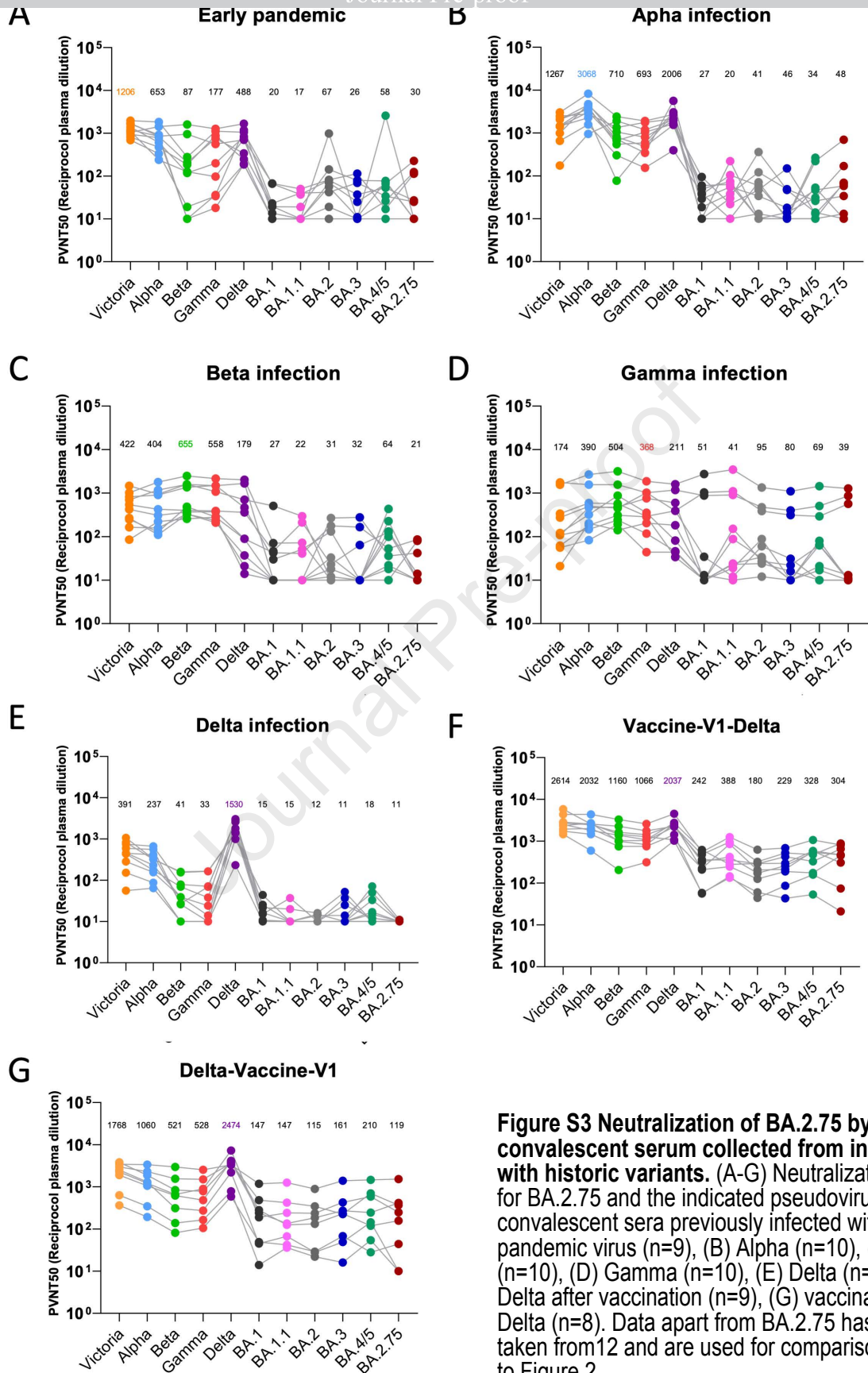


**Figure S3 Neutralization of BA.2.75 by panels of convalescent serum collected from infection with historic variants.** (A-G) Neutralization titres for BA.2.75 and the indicated pseudoviruses using convalescent sera previously infected with (A) Early pandemic virus (n=9), (B) Alpha (n=10), (C) Beta (n=10), (D) Gamma (n=10), (E) Delta (n=10), (F) Delta after vaccination (n=9), (G) vaccination after Delta (n=8). Data apart from BA.2.75 has been taken from 12 and are used for comparison. Related to Figure 2.

**Table S1** Journal Pre-proof  
**PV including BA.2.75 and BA.2+N460K (related to Figure 5A)**

mAbs	Victoria	BA.1	BA.1.1	BA.2	BA.3	BA.4/5	BA.2.75	BA.2+N460K
Omi-02	0.002 ± 0.001	0.004 ± 0.001	0.004 ± 0.001	0.003 ± 0.001	0.019 ± 0.007	>10	0.009 ± 0.002	0.025 ± 0.003
Omi-03 (3-53)	0.003 ± 0.000	0.005 ± 0.002	0.003 ± 0.001	0.008 ± 0.001	0.022 ± 0.003	0.017 ± 0.005	0.017 ± 0.000	0.401 ± 0.026
Omi-06	0.007 ± 0.000	0.017 ± 0.003	0.139 ± 0.033	0.039 ± 0.008	0.696 ± 0.106	>10	0.063 ± 0.005	0.026 ± 0.002
Omi-08	0.008 ± 0.004	0.003 ± 0.000	0.002 ± 0.000	0.114 ± 0.045	0.032 ± 0.001	0.086 ± 0.005	0.036 ± 0.002	0.552 ± 0.090
Omi-09	0.006 ± 0.002	0.005 ± 0.000	0.005 ± 0.002	0.008 ± 0.002	0.017 ± 0.002	0.166 ± 0.007	0.003 ± 0.000	0.010 ± 0.002
Omi-12	0.006 ± 0.002	0.002 ± 0.000	0.002 ± 0.001	0.003 ± 0.001	0.006 ± 0.001	0.429 ± 0.060	0.003 ± 0.001	0.011 ± 0.002
Omi-16 (3-66)	0.014 ± 0.003	0.012 ± 0.002	0.011 ± 0.003	0.034 ± 0.012	0.111 ± 0.008	0.029 ± 0.007	>10	>10
Omi-17 (3-66)	0.023 ± 0.011	0.018 ± 0.012	0.022 ± 0.009	0.060 ± 0.004	0.123 ± 0.002	0.028 ± 0.001	0.255 ± 0.169	>10
Omi-18 (3-53)	0.008 ± 0.003	0.002 ± 0.000	0.002 ± 0.000	0.005 ± 0.000	0.006 ± 0.002	0.005 ± 0.001	0.035 ± 0.007	0.014 ± 0.002
Omi-20 (3-66)	0.009 ± 0.002	0.006 ± 0.001	0.005 ± 0.001	0.015 ± 0.003	0.020 ± 0.004	0.014 ± 0.006	0.178 ± 0.075	0.315 ± 0.142
Omi-23	0.005 ± 0.002	0.029 ± 0.006	0.023 ± 0.12	0.019 ± 0.005	0.011 ± 0.000	>10	0.011 ± 0.006	0.022 ± 0.005
Omi-24	0.005 ± 0.000	0.006 ± 0.002	0.054 ± 0.015	0.007 ± 0.001	0.009 ± 0.002	>10	0.008 ± 0.004	0.014 ± 0.000
Omi-25	0.005 ± 0.001	0.023 ± 0.005	0.027 ± 0.005	0.024 ± 0.004	0.050 ± 0.004	>10	0.014 ± 0.005	0.050 ± 0.010
Omi-26	0.002 ± 0.001	0.006 ± 0.002	0.005 ± 0.001	0.013 ± 0.001	0.018 ± 0.002	>10	0.010 ± 0.004	0.010 ± 0.000
Omi-27 (3-66)	0.008 ± 0.003	0.026 ± 0.006	0.034 ± 0.009	0.034 ± 0.005	0.026 ± 0.007	0.069 ± 0.023	6.672 ± 4.466	>10
Omi-28 (3-66)	0.022 ± 0.000	0.011 ± 0.004	0.009 ± 0.002	0.008 ± 0.000	0.019 ± 0.000	0.028 ± 0.009	0.133 ± 0.082	0.103 ± 0.048
Omi-29 (3-53)	0.014 ± 0.006	0.017 ± 0.003	0.016 ± 0.009	0.056 ± 0.014	0.064 ± 0.017	0.396 ± 0.007	>10	>10
Omi-30	0.012 ± 0.002	0.008 ± 0.003	0.008 ± 0.004	0.011 ± 0.002	0.015 ± 0.003	>10	0.008 ± 0.002	0.018 ± 0.001
Omi-31	0.376 ± 0.090	0.029 ± 0.002	0.031 ± 0.012	0.013 ± 0.002	0.013 ± 0.004	>10	0.014 ± 0.008	0.015 ± 0.001
Omi-32	0.010 ± 0.006	0.017 ± 0.000	>10	2.682 ± 0.553	1.018 ± 0.139	0.035 ± 0.016	0.354 ± 0.064	2.341 ± 0.282
Omi-33	0.027 ± 0.011	0.014 ± 0.005	0.042 ± 0.018	0.068 ± 0.022	0.133 ± 0.021	0.013 ± 0.004	0.053 ± 0.006	0.490 ± 0.156
Omi-34	0.007 ± 0.004	0.008 ± 0.001	0.062 ± 0.004	0.009 ± 0.003	0.014 ± 0.000	>10	0.005 ± 0.000	0.020 ± 0.001
Omi-35	0.018 ± 0.004	0.058 ± 0.006	0.381 ± 0.061	0.094 ± 0.004	0.044 ± 0.018	1.687 ± 0.441	0.020 ± 0.000	0.056 ± 0.012
Omi-36 (3-66)	0.022 ± 0.004	0.009 ± 0.003	0.009 ± 0.003	0.030 ± 0.014	0.178 ± 0.048	0.024 ± 0.006	>10	>10
Omi-38	0.015 ± 0.004	0.024 ± 0.015	>10	0.005 ± 0.000	0.008 ± 0.002	0.005 ± 0.001	0.011 ± 0.005	0.010 ± 0.001
Omi-39	0.014 ± 0.002	0.009 ± 0.004	>10	0.026 ± 0.011	0.014 ± 0.001	0.035 ± 0.003	0.027 ± 0.009	0.045 ± 0.017
Omi-41	>10	0.053 ± 0.028	0.037 ± 0.002	>10	0.032 ± 0.007	>10	>10	>10
Omi-42	0.013 ± 0.004	0.007 ± 0.004	0.006 ± 0.002	0.021 ± 0.011	0.025 ± 0.012	0.013 ± 0.001	0.003 ± 0.000	0.007 ± 0.002

**(B) IC50 of commercial mAbs against PV BA.2.75 (related to Figure 5B)**

	IC50 (µg/mL)						
	Victoria	BA.1	BA.1.1	BA.2	BA.3	BA.4/5	BA.2.75
REGN10987	0.002 ± 0.001	>10	>10	0.616 ± 0.347	>10	>10	>10
REGN10933	0.001 ± 0.002	>10	>10	>10	>10	>10	>10
AZD1061	0.002 ± 0.001	0.308 ± 0.058	>10	0.008 ± 0.003	0.019 ± 0.007	0.015 ± 0.004	0.021 ± 0.002
AZD8895	0.001 ± 0.000	0.246 ± 0.027	0.100 ± 0.053	1.333 ± 0.317	>10	>10	0.008 ± 0.000
AZD7442	0.001 ± 0.000	0.232 ± 0.113	0.806 ± 0.093	0.008 ± 0.001	0.065 ± 0.011	0.065 ± 0.007	0.017 ± 0.003
ADG10	0.007 ± 0.002	>10	>10	>10	>10	>10	>10
ADG20	0.003 ± 0.002	0.348 ± 0.169	0.253 ± 0.070	>10	>10	>10	>10
ADG30	0.014 ± 0.006	>10	>10	>10	>10	>10	>10
Ly-CoV555	0.002 ± 0.000	>10	>10	>10	>10	>10	>10
Ly-CoV16	0.014 ± 0.010	>10	>10	>10	>10	>10	>10
Ly-CoV1404	0.001 ± 0.000	0.002 ± 0.000	0.001 ± 0.000	0.001 ± 0.000	0.002 ± 0.000	0.002 ± 0.000	0.002 ± 0.000
S309	0.079 ± 0.027	0.113 ± 0.006	0.142 ± 0.012	0.638 ± 0.154	0.311 ± 0.023	0.689 ± 0.041	0.202 ± 0.017

**Table S2. IC50 of BA.1 mAbs against PV BA.2, BA.2.75 and BA.2 with each of the four BA.2.75 mutations (see also Figure S1, related to Figure 5)**

mAbs	IC50 (µg/ml)					
	BA.2	BA.2+D339H	BA.2+R493Q	BA.2+G446S	BA.2.+ N460K	BA.2.75
Omi02	0.003 ± 0.000	0.007 ± 0.003	0.003 ± 0.000	0.007 ± 0.002	0.025 ± 0.003	0.009 ± 0.002
Omi03	0.008 ± 0.001	0.006 ± 0.000	0.002 ± 0.001	0.005 ± 0.001	0.401 ± 0.026	0.017 ± 0.000
Omi06	0.039 ± 0.008	0.012 ± 0.002	0.023 ± 0.010	0.087 ± 0.002	0.026 ± 0.002	0.063 ± 0.005
Omi08	0.114 ± 0.045	0.250 ± 0.009	0.194 ± 0.020	0.017 ± 0.001	0.552 ± 0.090	0.036 ± 0.002
Omi09	0.008 ± 0.002	0.005 ± 0.001	0.003 ± 0.000	0.006 ± 0.001	0.010 ± 0.002	0.003 ± 0.000
Omi12	0.003 ± 0.001	0.003 ± 0.001	0.001 ± 0.000	0.003 ± 0.001	0.011 ± 0.002	0.003 ± 0.001
Omi16	0.034 ± 0.012	0.014 ± 0.004	0.008 ± 0.003	0.018 ± 0.004	>10	>10
Omi17	0.060 ± 0.004	0.036 ± 0.015	0.013 ± 0.001	0.038 ± 0.002	>10	0.255 ± 0.169
Omi18	0.005 ± 0.000	0.003 ± 0.000	0.004 ± 0.000	0.003 ± 0.000	0.014 ± 0.002	0.035 ± 0.007
Omi20	0.015 ± 0.003	0.007 ± 0.000	0.005 ± 0.001	0.005 ± 0.001	0.315 ± 0.142	0.178 ± 0.075
Omi23	0.019 ± 0.005	0.006 ± 0.000	0.007 ± 0.000	0.010 ± 0.002	0.022 ± 0.005	0.011 ± 0.006
Omi24	0.007 ± 0.001	0.005 ± 0.001	0.004 ± 0.000	0.005 ± 0.000	0.014 ± 0.000	0.008 ± 0.004
Omi25	0.024 ± 0.004	0.016 ± 0.003	0.007 ± 0.002	0.022 ± 0.000	0.050 ± 0.010	0.014 ± 0.005
Omi26	0.013 ± 0.001	0.007 ± 0.002	0.008 ± 0.001	0.008 ± 0.002	0.010 ± 0.000	0.010 ± 0.004
Omi27	0.034 ± 0.006	0.007 ± 0.001	0.007 ± 0.001	0.011 ± 0.001	>10	6.672 ± 4.466
Omi28	0.008 ± 0.000	0.009 ± 0.001	0.010 ± 0.001	0.014 ± 0.000	0.103 ± 0.048	0.133 ± 0.082
Omi29	0.056 ± 0.014	0.018 ± 0.006	0.042 ± 0.012	0.024 ± 0.002	>10	>10
Omi30	0.013 ± 0.002	0.006 ± 0.001	0.002 ± 0.000	0.003 ± 0.000	0.018 ± 0.001	0.008 ± 0.002
Omi31	0.011 ± 0.002	0.005 ± 0.001	0.003 ± 0.000	0.005 ± 0.001	0.015 ± 0.001	0.014 ± 0.008
Omi32	2.614 ± 0.533	0.683 ± 0.179	0.312 ± 0.008	0.330 ± 0.010	2.341 ± 0.282	0.354 ± 0.064
Omi33	0.070 ± 0.024	0.177 ± 0.035	0.063 ± 0.008	0.043 ± 0.016	0.490 ± 0.156	0.053 ± 0.006
Omi34	0.009 ± 0.003	0.004 ± 0.000	0.002 ± 0.000	0.002 ± 0.000	0.020 ± 0.001	0.005 ± 0.000
Omi35	0.092 ± 0.004	0.012 ± 0.003	0.017 ± 0.011	0.014 ± 0.006	0.056 ± 0.012	0.020 ± 0.000
Omi36	0.030 ± 0.014	0.036 ± 0.002	0.013 ± 0.003	0.067 ± 0.015	>10	>10
Omi38	0.005 ± 0.000	0.011 ± 0.000	0.003 ± 0.001	0.010 ± 0.000	0.010 ± 0.001	0.011 ± 0.005
Omi39	0.026 ± 0.011	0.012 ± 0.002	0.021 ± 0.007	0.009 ± 0.002	0.045 ± 0.017	0.027 ± 0.009
Omi41	>10	>10	>10	>10	>10	>10
Omi42	0.021 ± 0.011	0.011 ± 0.002	0.006 ± 0.001	0.016 ± 0.002	0.007 ± 0.002	0.003 ± 0.000

	De V1-Vaccine	Vac e-V1_Delta	Delta	Gamma	Beta	Alpha	E y pandemic	BN 52b2 V3+28	AZ V3+28	B /5 infection	.2 infection	.1 infection
<b>Participants</b>												
Female	7	7	7	7	7	7	7	7	7	7	7	7
Male	4	4	3	4	5	6	9	10	21	5	4	7
Median Age (Y)	41 (Range 31-54)	40 (Range 28-70)	26 (Range 12-36)	32 (Range 23-49)	47 (Range 16-64)	57 (Range 29-76)	60 (Range 53-69)	45 (Range 30-59)	37 (Range 25-53)	42 (Range 20-94)	41 (Range 22-57)	22 (Range 21-56)

Table S3. Sample participant information.

**Table S4.** Primers used for site-directed PCR mutagenesis to generate the BA.2.75 construct using the BA.2 Spike construct as template (related to methods)

Primer ID	Sequence
D339H_pNeoF	5' -GGTTGCGTAGCTGAAACCGGTACCAATCTGTGCCCTTCCACGAGGTGTTCAATGCCACC-3'
G446S_F	5' -CAAAC TAGATTGCGAAAGTTAGCGGCAATTACAATTACCTG-3'
G446S_R	5' -CAGGTAATTGTAATTGCCGCTAACTTTCGAATCTAGTTTG-3'
N460K_F	5' -CAGACTGTTTCAGAAAGAGCAAACCTGAAGCCTTTCGAGAGAGAC-3'
N460K_R	5' -GTCTCTCTCGAAAGGCTTCAGTTTGCTCTTCTGAACAGTCTG-3'
R493Q_F (RBD)	5' -CAATTGCTACTTCCCTCTGCAGAGCTACGGCTTCAGACCTACC-3'
R493Q_R (RBD)	5' -GGTAGGTCTGAAGCCGTAGCTCTGCAGAGGGAAGTAGCAATTG-3'
RBD333_BAP_R	5' -GTCATTCAGCAAGCTCTTCTTGCCGCACACGGTAGC-3'
pNeoRBD333Omi_F	5' -GGTTGCGTAGCTGAAACCGGTCATCACCATCACCATCACCCAATCTGTGCCCTTTCGAC-3'
K147E_W152R_F157L_F	5' -CGTTTATTATCATGAGAACAACAAGAGCAGGATGGAGAGCGAGTTACGCGTATATTCGTCGGC-3'
K147E_W152R_F157L_R	5' -GCCGACGAATATACGCGTAACTCGCTCTCCATCCTGCTCTTGTGTTCTCATGATAATAAACG-3'
I210L_F	5' -CAGCAAGCACACACCCGTTAATCTGGGCAGAGACC-3'
I210L_R	5' -GGTCTCTGCCAGATTAACGGGTGTGTGCTTGCTG-3'
G275S_F	5' -GCGATTTCGCAAGCAGTTGGACCCGCTGGAGC-3'
G275S_R	5' -GCTCCAGCGGTCCAACCTGCTTGACGAATCGC-3'
D339H_F	5' -CAATCTGTGCCCTTCCACGAGGTGTTCAATGC-3'
D339H_R	5' -GCATTGAACACCTCGTGAAAGGGCAGATTG-3'
G446S_N460K_F	5' -GAACTCTAACAACTAGATTCGAAAGTTAGCGGCAATTACAATTACCTGTACAGACTGTTTCAGAAAGAGCAAGCTGAAGCCTTTCGAGAG-3'
G446S_N460K_R	5' -CTCTCGAAAGGCTTCAGCTTGCTCTTCTGAACAGTCTGTACAGGTAATTGTAATTGCCGCTAACTTTCGAATCTAGTTTGTAGAGTTC-3'
R493Q_F	5' -GCTTCAATTGCTACTTCCCTCTGCAGAGCTACGGCTTCAGACCTACC-3'
R493Q_R	5' -GGTAGGTCTGAAGCCGTAGCTCTGCAGAGGGAAGTAGCAATTGAAGC-3'

**Table S5. X-ray data collection and structure refinement statistics (related to Figure 4)**<sup>a</sup> Values in parentheses are for highest-resolution shell.

Structure	BA.2.75 RBD/ACE2
PDB ID	8ASY
Data collection	
Space group	P4 <sub>1</sub> 2 <sub>1</sub> 2
Cell dimensions	
a, b, c (Å)	105.3, 105.3, 220.8
a, b, g (°)	90, 90, 90
Resolution (Å)	76–2.85 (2.80–2.85) <sup>a</sup>
R <sub>merge</sub>	0.443 (---)
R <sub>pim</sub>	0.086 (1.401)
I/s(I)	7.6 (0.4)
CC <sub>1/2</sub>	0.971 (0.279)
Completeness (%)	99.8 (96.9)
Redundancy	26.8 (25.7)
Refinement	
Resolution (Å)	76–2.85
No. reflections	2089/1439
R <sub>work</sub> / R <sub>free</sub>	0.217/0.265
No. atoms	
Protein	6464
Ligand/ion/water	167
B factors (Å <sup>2</sup> )	
Protein	86
Ligand/ion/water	108
r.m.s. deviations	
Bond lengths (Å)	0.002
Bond angles (°)	0.4